ON THE HYDRODYNAMIC FORCES AND MOMENTS ACTING ON THE TWO DIMENSIONAL BODIES OSCILLATING IN SHALLOW WATER

Takaki, Mikio
Research Institute for Applied Mechanics, Kyushu University : Research Associate

https://doi.org/10.5109/6610205

出版情報：Reports of Research Institute for Applied Mechanics. 25 (78), pp.1-64, 1977-09. 九州大学応用力学研究所

Reports of Research Institute for Applied Mechanics
Vol. XXIV, No. 78, 1977

ON THE HYDRODYNAMIC FORCES AND MOMENTS ACTING ON THE TWO DIMENSIONAL BODIES OSCILLATING IN SHALLOW WATER*

By Mikio TAKAKI**

This paper presents the solutions of radiation problems and the diffraction problems in water of finite depth. The hydrodynamic forces and moments acting on the cylinders of the arbitrary cross sections are calculated precisely by adopting the close fit method.

In the next place, the forced oscillating tests for heave, sway and roll are carried out by using three cylinders of Lewis form cross section. It becomes clear from the comparison with the experimental results that the two dimensional hydrodynamic forces and moments acting on the arbitrary cross sections without bilgekeel can be precisely obtained by the close fit method.

Finally numerical examples for submerged circular cylinder are shown. And the effects of water depth and the viscous effects for roll are discussed.

1. Introduction

Because of increasing dimensions of ship in recent years, several sea depths of her trade routs and her working area have been becoming relatively shallow. The reduction of sea depth may lead to hit or grand the bottom of sea. It therefore has been becoming a great important problem to predict the ship motions and the hydrodynamic forces acting on the ships in water of finite depth, in which the ships can operate safely.

When the strip method is available for predicting the motions of ships in water of finite depth, the two dimensional hydrodynamic forces and moments acting on the body of ship are required according to the assumption of the strip theory. As for the calculating methods of the hydrodynamic forces and moments acting on the two dimensional oscillating body in water of finite depth, Porter discussed about the hydrodynamic forces acting on the heaving cylinder [1]. Yu and Ursell calculated the added mass and the wave

---

* This paper is translated from two papers which have been published at the Society of Naval Architects of West-Japan on May 1975 and 1976.

** Research Associate, Research Institute for Applied Mechanics, Kyushu University

amplitude ratio of the heaving semi-circular cylinder and confirmed the availability of their calculated values by the experiment of the wave amplitude ratio for heave [2]. Sayer and Ursell obtained the added mass coefficients of heaving semi-circular cylinder at $\omega \to 0$ by numerical calculations [3]. C. H. Kim [4] and H. Keil [5] independently calculated the hydrodynamic forces and moments acting on the Lewis form cylinder for heave, sway and roll by adopting the method of multipole expansions which was an extension of the method of Grim [6] and Tamura [7] of the water of infinite depth to that of the water of finite depth. Black & others [8] and Ijima & others [9] solved the radiation problem of the rectangular cylinder by using the method of dividing the fluid domain. These methods above mentioned contain a weakpoint, by which is limited the shapes of sections of the ships or the structures. There exist on the contrary the finite element method and the close fit method which do not limit the shapes of cross sections to calculate the hydrodynamic forces and moments acting on those. As for the finite element method, K. J. Bai [10,11], Seto & Yamamoto [12,13] and Takashina & others [14] solved the radiation problems. As for the close fit method, Maruyama [15], Kan [16][17] and Ikebuchi [18] obtained the two dimensional hydrodynamic forces and moments in water of finite depth.

As mentioned above, especially there have been few experimental results. Consequently the correlation works between the theoretical and the experimental investigations have been scarcely performed.

In this paper, firstly we shall extend the relations [19] among the hydrodynamic forces in the case of water of infinite depth to those in the case of water of finite depth using the potential [20] of water of finite depth, and solve the radiation problems and the diffraction problems on arbitrary two dimensional cross section using the close fit method in which singularities are distributed on the surface of the cylinder. The hydrodynamic forces and moments acting on an arbitrary cross section are calculated precisely by using the above method.

In the next place, the forced oscillating tests are carried out by using three cylinders of Lewis form cross section, and the experimental results concerning added mass coefficients, damping force coefficients and wave amplitude ratios are compared with the theoretically calculated results obtained by the close fit method. The availability of the theoretically calculating method is confirmed experimentally.

Finally we shall discuss the effects of water depths as for the hydrodynamic forces and moments.

1.1 Notation

L	Length of cylinder
B	Breadth of cross section C
T	Draft

Δ	Volume displacement of cross section
A_W	Water plane area
C_B	Block coefficient
$\overline{GM}$	Metacentric height
k_t	Radius of transverse gyration for roll
$b_{B.K.}$	Breadth of bilge-keel
C	Submerged part of cross sectional contour in rest position
ds	Line segment along cross sectional contour
n	Unit normal to cross section C
H_0	Beam draft ratio $(=B/2T)$
σ	Sectional area coefficient $(=\Delta/BT)$
g	Gravitational acceleration
KT	Non-dimensional frequency $(=\frac{\omega^2}{g}T)$
ρ	Density of fluid
h	Depth of fluid
ω	Circular frequency of wave
K	Wave number in water of infinite depth $(=\frac{\omega^2}{g})$
m_0	Wave number in water of finite depth (a real root of equation: $\frac{\omega^2}{g}=m_0 \tanh m_0 h$)
n_j, $(j=1, 2, 3\cdots)$	Imaginary roots of equation: $\frac{\omega^2}{g}=m_0 \tanh m_0 \mathrm{h}$
ζ_a	Amplitude of incident wave
$\eta(x,y;\ t)$, $\hat{\eta}(x,y)$	Amplitude of outgoing wave
Y_j	Oscillation amplitude in the j-th mode
$\phi_j(x,y;\ x',\ y')$	Velocity potential normalized by velocity amplitude in the j-th mode motion $(j=1,2,3)$ Velocity potential normalized by amplitude of incident wave $(j=0,4)$
$\psi_j(x,y;\ x',\ y')$	Stream function corresponding to velocity potential
$\sigma_j(x,y)$	Density of source singularities distributed on sectional contour
c_j	Integral constant for the j-th mode equation
F_{jk}, f_{jk}	Hydrodynamic force or moment of the k-th mode by the j-th mode of motion
E_j, e_j	Wave exciting force or moment of the j-th mode in beam-sea condition
P_j	Pressure of the j-th mode
$\hat{M}_H, \hat{M}_S, \hat{M}_R$	Added mass coefficient for heave, sway and added mass moment of inertia coefficient for roll
$\hat{N}_H, \hat{N}_S, \hat{N}_R$	Damping coefficient for heave, sway and roll

$\hat{A}_H$, $\hat{A}_S$, $\hat{A}_R$	Wave amplitude ratio for heave, sway and roll (Amplitude of radiation wave normalized by amplitude of oscillation)
l_{SR}	Lever of added moment of inertia
l_w	Lever of damping moment
J_ϕ	Mass moment of inertia for roll
ε_j	Phase lag on the j-th mode
Subscripts	
c	Real part
s	Imaginary part
A	Symmetric motion
B	Antisymmetric motion
1	Motion along x-axis (swaying mode)
2	Motion along y-axis (heaving mode)
3	Rotation around the origin O (rolling mode)
4	Diffraction wave
0	Incident wave

2. Formulation of fundamental problems

2.1 Coordinate systems

Consider a cylinder, whose cross section C is symmetrical about a center

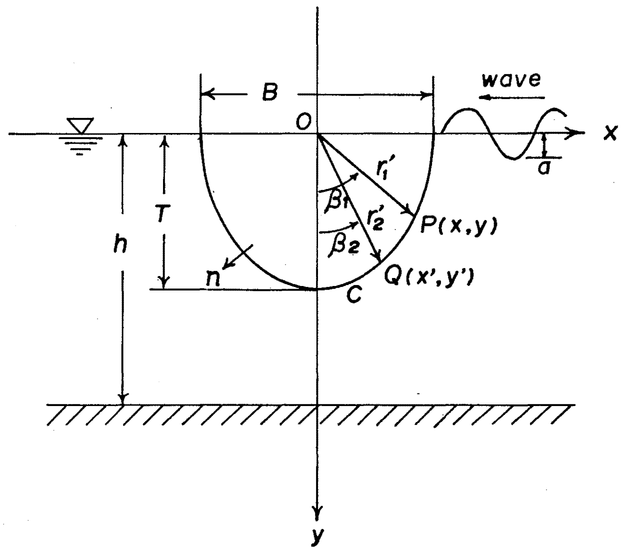

Fig. 2.1 Coodinate system

line, which is forced into a simple harmonic oscillation with a small amplitude in water of finite depth as shown in Fig. 2. 1. Let a horizontal axis, which coincides with an undisturbed free surface, be x-coordinate axis and a virtical axis be y-coordinate axis, which is measured downwards, and a normal direction n on hull surface be directed into fluid. Considering the motions of fluid with a constant depth h to be linear and two dimensional phenomena, it is assumed that the fluid is invisid, imcompressible and irrotational, and the effect of surface tension is negligible.

2. 2 Fundamental equations

Let the velocity potential Φ, the pressure P and the displacement of free surface η be represented as follows:

$$\begin{aligned}\Phi(x,y;\mathrm{t}) &= Re\{\phi(x,y)\mathrm{e}^{i\omega t}\},\\ P(x,y;t) &= Re\{p(x,y)\mathrm{e}^{i\omega t}\},\\ \eta(x,y;t) &= Re\{\hat{\eta}(x,y)\mathrm{e}^{i\omega t}\}.\end{aligned} \tag{2. 1}$$

and we have the relation between wave frequency ω and wave number m_0 in fluid of finite depth:

$$K=\frac{\omega^2}{g}=m_0 \tanh m_0 h. \tag{2. 2}$$

Furthermore, let the unite velocity potential $\phi_j(x,y)$ with respect to radiation potential $\varphi\ (x,y)$ oscillating with the amplitude Y_j be put as follows:

$$\varphi_j(x,y)=i\omega\phi_j Y_j,\ (j=1,2,3), \tag{2. 3}$$

where ϕ_j satisfies:

[L] the Laplace equation, in the fluid domain:

$$\frac{\partial^2\phi_j}{\partial x^2}+\frac{\partial^2\phi_j}{\partial y^2}=0, \tag{2. 4}$$

[S] the dynamic free surface condition:

$$K\phi_j+\left.\frac{\partial\phi_j}{\partial y}\right|_{y=0}=0, \tag{2. 5}$$

[B] the water bottom condition:

$$\left.\frac{\partial\phi_j}{\partial y}\right|_{y=h}=0, \tag{2. 6}$$

[R] the radiation condition:

$$\lim_{x\to\pm\infty}\left(\frac{\partial\phi_j}{\partial x}\pm im_0\phi_j\right)\sim 0, \tag{2. 7}$$

[N] the ship hull condition:

$$\frac{\partial \phi_j}{\partial n} = v_{nj}, \qquad \text{on } C, \ (j=1,2,3) \tag{2.8}$$

where v_{nj} are normal components of velocity on ship hull and can be expressed as follows:

$$v_{n1} = -\frac{\partial x}{\partial n}, \quad v_{n2} = -\frac{\partial y}{\partial n}, \quad v_{n3} = y\frac{\partial x}{\partial n} - x\frac{\partial y}{\partial \mathrm{n}}. \tag{2.9}$$

Rewriting the equation (2.9) by using the stream function ψ_j conjugated with the velocity potential ϕ_j,
we have

$$\psi_1 = -y + c_1, \quad \psi_2 = x + c_2, \quad \psi_3 = \frac{1}{2}(x^2+y^2) + c_3, \tag{2.10}$$

where $c_j(j=1,2,3)$ is unknown constant.

The velocity potential of incident wave and reflective wave can be put as follows:

$$\varphi_{0,4}(x,y) = \frac{ig}{\omega} a \cdot \phi_{0,4}(x,y), \tag{2.11}$$

where a is wave amplitude, and then we have

$$\frac{\partial}{\partial n}(\phi_0 + \phi_4) = 0, \tag{2.12}$$

on the hull surface C. The pressures with respect to the radiation potential and the diffraction potential can be expressed as follows:

$$p = -\rho\omega^2 Y_j \phi_j, \quad (j=1,2,3), \tag{2.13}$$

$$p = -\rho g a(\phi_0 + \phi_4), \tag{2.14}$$

and the displacement of free surface with respect to the radiation potential can be expressed as follows:

$$\hat{A}\mathrm{j} = \frac{\hat{\eta}_j}{Y_j} = K\phi_j|_{y=0}, \quad (j=1,2,3). \tag{2.15}$$

2.3 Velocity potential and stream function

When a periodic source with a unite strength is put at an arbitrary point (x', y') in water of finite depth, the velocity potential, which satisfies conditions (2.4)$\sim$(2.7), at the point $P(x,y)$ have been given by Thorne[19] as

$$G(x,y;\ x',y') = G_c(x,y;\ x',y') + iG_s(x,y;\ x',y')$$

$$= \log\frac{r_1}{r_2} + 2\cdot\mathrm{P.V.}\int_0^\infty \left\{ \frac{\cosh k(h-y)\ \cosh k(h-y')}{(K\cosh kh - k\sinh kh)\ \cosh kh} \right.$$

$$-\frac{e^{-kh}\sinh ky \sinh ky'}{k\cosh kh}\Big\}\cos k(x-x')dk \qquad (2.16)$$

$$+i\frac{4\pi\cosh m_0(h-y)\cosh m_0(h-y')}{2m_0h+\sinh 2m_0h}\cos m_0(x-x'),$$

where $\quad r_1=\sqrt{(x-x')^2+(y-y')^2}, \quad r_2=\sqrt{(x-x')^2+(y+y')^2}.$

And the stream function, which is conjugated with equation (2.16), can be expressed as

$$S(x,y;\ x',y')=S_c(x,y;\ x',y')+iS_s(x,y;\ x',y')$$

$$=\theta_1-\theta_2+2\cdot\text{P.V.}\int_0^\infty\Big\{\frac{\sinh k(h-y)\cosh k(h-y')}{(K\cosh kh-k\sinh kh)\cosh kh}$$

$$+\frac{e^{-kh}\cosh ky\sinh ky'}{k\cosh kh}\Big\}\sin k(x-x')dk \qquad (2.17)$$

$$+i\frac{4\pi\sinh m_0(h-y)\cosh m_0(h-y')}{2m_0h+\sinh 2m_0h}\sin m_0(x-x').$$

3. Two dimensional boundary-value problems

3.1 Integral equations and solutions

Distributing line density of source $\sigma_j(j=1,2,3)$ on the surface of cylinder, the velocity potential and the stream function at an arbitrary point $P(x, y)$ in fluid can be expressed as follows:

$$\phi_j(x,y)=\int_c\sigma_j(x',y')\cdot G(x,y;\ x',y')ds(x',y'), \quad (j=1,2,3), \qquad (3.1)$$

$$\psi_j(x,y)=\int_c\sigma_j(x',y')\cdot S(x,y;\ x',y')ds(x',y'), \quad (j=1,2,3). \qquad (3.2)$$

Solving these integral eqations and evaluating the line density of source σ_j, the velocity potential function can be obtained. It is, however, complicated to perform the numerical calculations of equation (3.1) involving differentiations on these velocity potential. So we should evaluate the line density of source $\sigma_j(x, y)$ by using the stream function (3.2). Rewrite equation (3.2) by dividing into a real part and an imaginary part, the following equations can be obtained:

$$\left.\begin{aligned}\psi_{jc}(P)&=\int_c\{\sigma_{jc}(Q)\cdot S_c(P,Q)-\sigma_{js}(Q)\cdot S_s(P,Q)\}ds(Q),\\ \psi_{js}(P)&=\int_c\{\sigma_{jc}(Q)\cdot S_s(P,Q)+\sigma_{js}(Q)\cdot S_c(P,Q)\}ds(Q),\ (j=1,2,3).\end{aligned}\right\} \qquad (3.3)$$

One can evaluate σ_{jc} and σ_{js} by solving these two sets of integral equations, but in the case of symmetrical cross section of cylinder, one can symplify the numerical calculations as follows [21].

The case of symmetrical motion ($j=2$, heave): There are following relations given by

$$\sigma_2(x',y')=\sigma_2(-x',y'),\quad S_s(x,y;\ x',y')=S_s(x,y;\ -x',y'),$$

and the imaginary part of stream function can be obtained as

$$S_s(P,Q)=\frac{4\pi\ \sinh\ m_0(h-y)}{2m_0h+\sinh\ 2m_0h}\sin\ m_0x\cdot\cosh\ m_0(h-y')\ \cos\ m_0x'. \tag{3.4}$$

The case of anti-symmetrical motions ($j=1$, sway; $j=3$, roll): There are following relations given by

$$\sigma_j(x',y')=-\sigma_j(-x',y'),\ (j=1,3),\quad S_s(x,y;\ x',y')=-S_s(x,y;\ -x',y'),$$

and the imaginary part of stream function can be expressed as follows:

$$S_s(P,Q)=-\frac{4\pi\ \sinh\ m_0(h-y)}{2m_0h+\sinh\ 2m_0h}\cos\ m_0x\ \cosh\ m_0(h-y')\ \sin\ m_0x'. \tag{3.5}$$

We consider the following functions given by

$$\left.\begin{aligned}\begin{Bmatrix}P_{2c}\\P_{jc}\end{Bmatrix}&=\int_c\begin{Bmatrix}\sigma_{2c}(x',y')\cdot\cos\ m_0x'\\\sigma_{jc}(x',y')\cdot\sin\ m_0x'\end{Bmatrix}\frac{\cosh\ m_0(h-y')}{\cosh\ m_0h}ds(x',y'),\\ \begin{Bmatrix}P_{2s}\\P_{js}\end{Bmatrix}&=\int_c\begin{Bmatrix}\sigma_{2s}(y',y')\cdot\cos\ m_0x'\\\sigma_{js}(x',y')\cdot\sin\ m_0x'\end{Bmatrix}\frac{\cosh\ m_0(h-y')}{\cosh\ m_0h}ds(x',y'),\ (j=1,3),\end{aligned}\right\} \tag{3.6}$$

and

$$\left.\begin{aligned}\sigma_{jA}(x',y')&=\sigma_{jc}(x',y')+\frac{P_{js}}{P_{jc}}\sigma_{js}(x',y'),\\ \sigma_{jB}(x',y')&=\frac{1}{P_{jc}}\sigma_{js}(x',y'),\qquad (j=1,2,3),\end{aligned}\right\} \tag{3.7}$$

and so equation (3.3) can be transformed into the following forms:

$$\left.\begin{aligned}&\begin{Bmatrix}\phi_{2c}\\\phi_{jc}\end{Bmatrix}=\int_c\begin{Bmatrix}\sigma_{2A}(x',y')\\\sigma_{jA}(x',y')\end{Bmatrix}S_c(x,y;\ x',y')ds(x',y'),\\ &\frac{4\pi\ \sinh m_0(h-y)\ \cosh m_0h}{2m_0h+\sinh\ 2m_0h}\cdot\begin{Bmatrix}(-\sin\ m_0x)\\\cos\ m_0x\end{Bmatrix}+\begin{Bmatrix}0\\\phi_{js}\end{Bmatrix}=\\ &\int_c\begin{Bmatrix}\sigma_{2B}(x',y')\\\sigma_{jB}(x',y')\end{Bmatrix}S_c(x,y;\ x',y')ds(x',y')\quad (j=1,3).\end{aligned}\right\} \tag{3.8}$$

Solving the above equation (3.8), we can evaluate the values of σ_{jA} and σ_{jB} ($j=1,2,3$). In the next place, we take the following functions given by:

$$\left.\begin{aligned} P_{jA}&=P_{jc}+\frac{P^2_{js}}{P_{jc}}, \\ P_{jB}&=\frac{P_{js}}{P_{jc}}, \qquad (j=1,2,3). \end{aligned}\right\} \tag{3.9}$$

The above equations (3.9) can be rewritten by the values of σ_{jA} and σ_{jB}, ($j=1,2,3$) as follows:

$$\left.\begin{aligned} \left.\begin{matrix} P_{2A} \\ P_{jA} \end{matrix}\right\} &= \int_c \left\{\begin{matrix} \sigma_{2A}(x',y') \cos m_0 x' \\ \sigma_{jA}(x',y') \sin m_0 x' \end{matrix}\right\} \frac{\cosh m_0(h-y')}{\cosh m_0 h} ds(x',y'), \\ \left.\begin{matrix} P_{2B} \\ P_{jB} \end{matrix}\right\} &= \int_c \left\{\begin{matrix} \sigma_{2B}(x',y') \cos m_0 x' \\ \sigma_{jB}(x',y') \sin m_0 x' \end{matrix}\right\} \frac{\cosh m_0(h-y')}{\cosh m_0 h} ds(x',y'), \quad (j=1,3). \end{aligned}\right\} \tag{3.10}$$

Substituting these relations into equations (3.9), we have:

$$\left.\begin{aligned} P_{jc}&=\frac{P_{jA}}{1+P^2_{jB}}, \\ P_{js}&=P_{jc}\cdot P_{jB}, \qquad (j=1,2,3) \end{aligned}\right\} \tag{3.11}$$

Furthermore the distributions of sources densities $\sigma_j(x',y')$ oscillating with the j-th mode can be obtained by the relations of equations (3.7) and (3.11) as follows:

$$\left.\begin{aligned} \sigma_{jc}(x',y')&=\sigma_{jA}(x',y')-P_{js}\cdot\sigma_{jB}(x',y') \\ \sigma_{js}(x',y')&=P_{jc}\cdot\sigma_{jB}(x',y'), \qquad (j=1,2,3). \end{aligned}\right\} \tag{3.12}$$

Substituting these values (3.12) into equation (3.1), the radiation potential functions can be obtained.

3.2 Integration of pressures

Since the hydrodynamical force of the k-th mode by the j-th mode of motion may be defined as $F_{jk}e^{i\omega t}$, the force normalized by the velocity amplitude can be represented as follows:

$$\left.\begin{aligned} f_{jk}&=\frac{F_{jk}}{\rho\omega^2 Y_j}=-\int_c \phi_j \frac{\partial \phi_k}{\partial n} ds, \\ f_{jk}&=f_{jkc}+if_{jks}, \qquad (j,k=1,2,3). \end{aligned}\right\} \tag{3.13}$$

These coefficients of hydrodynamical forces are shown in Table-3.1 and defined as follows:

In the case: $j=k$

the coefficient f_{jjc} expresses the added mass or the added mass moment of inertia,

the coefficient f_{jjs} expresses the damping force or the damping moment.

In the case: $j \neq k$

the coefficient f_{jkc} and f_{jks} express the coupling force or the coupling moment.

Table 3-1 Hydrodynamic force & moment and the non-dimensional coefficients

		Heave ($j=2$)	Sway ($j=1$)	Roll ($j=3$)
Force & Moment	Inertial force	$M_H=\rho f_{22c}$	$M_s=\rho f_{11c}$	$M_{\phi\eta}=\rho f_{31c}$
	Damping force	$N_H=-\rho\omega f_{22s}$	$N_s=-\rho\omega f_{11s}$	$N_{\phi\eta}=-\rho\omega f_{31s}$
	Inertial moment		$M_{\eta\phi}=\rho f_{13c}$	$M_R=\rho f_{33c}$
	Damping moment		$N_{\eta\phi}=-\rho\omega f_{13s}$	$N_R=-\rho\omega f_{33s}$
Non-dimensional coefficients	Added mass coeff.	$\hat{M}_H=M_H/\rho\varDelta$	$\hat{M}_S=M_S/\rho\varDelta$	
	Added mass m. t. of inertia coeff.			$\hat{M}_R=M_R/\rho\varDelta T^2$
	Damping force coeff.	$\hat{N}_H=\dfrac{N_H}{\rho\varDelta}\sqrt{B/2g}$	$\hat{N}_S=\dfrac{N_S}{\rho\varDelta}\sqrt{B/2g}$	
	Damping moment coeff.			$\hat{N}_R=\dfrac{N_R}{\rho\varDelta B^2}\sqrt{B/2g}$
	Wave amplitude ratio	$\hat{A}_H=\zeta_a/Y_2$	$\hat{A}_s=\zeta_a/Y_1$	$\hat{A}_R=\zeta_a/\phi_A T$
	Added moment arm		$\hat{l}_{SR}=\dfrac{M_{\eta\phi}}{M_S\cdot T}$	$\hat{l}_{RS}=\dfrac{M_{\phi\eta}}{M_S\cdot T}$
	Damping moment arm		$\hat{l}_w=\dfrac{N_{\eta\phi}}{N_S\cdot T}$	$\hat{l}_w=\dfrac{N_R}{N_{\phi\eta}\cdot T}$

3.3 Wave amplitude ratio

A group velocity of wave in water of finite depth can be expressed from the relation (2.2) as follows:

$$U=\frac{1}{2}\left(\frac{g}{m_0}\tanh m_0h\right)^{\frac{1}{2}}\cdot\left(1+\frac{2m_0h}{\sinh 2m_0h}\right). \tag{3.14}$$

Since the average total energy per unit surface area are expressed to be $\frac{1}{2}\rho g\hat{\eta}_j^2$, the average total energy of propagating wave per unit time E_0 can be expressed as

$$E_0=\frac{1}{2}\rho g\hat{\eta}_j^2\left(\frac{g}{m_0}\tanh\, m_0h\right)^{\frac{1}{2}}\cdot\left(1+\frac{2m_0h}{\sinh 2m_0h}\right),\quad (j=1,2,3). \tag{3.15}$$

Since this energy is equal to the average amount W_0 of work performed by the wave damping force acting on the cylinder, which is given by

$$W_0=\frac{1}{2}\rho\omega^3\ Y_j^2\ f_{jjs}, \tag{3.16}$$

the following equation can be obtained

$$\hat{A}_j^2=\frac{\hat{\eta}_j^2}{Y_j^2}=K^2\cdot F(m_0h)\,|\,f_{jjs}|,$$

$$\therefore A_j=K\{F(m_0h)\cdot|\,f_{jjs}|\}^{\frac{1}{2}},\quad (j=1,2,3), \tag{3.17}$$

where

$$F(m_0h)=\frac{2\cosh^2 m_0h}{2m_0h+\sinh 2m_0h}. \tag{3.18}$$

With aid of equations (3.13) and (3.17) the relation between the wave amplitude ratio $\hat{A}_j$ and the damping force coefficient N_j can be obtained as

$$\frac{N_j}{\rho\omega}=\frac{1}{F(m_0h)}\left|\frac{\hat{A}_j}{K}\right|^2,\quad (j=1,2,3). \tag{3.19}$$

This is the so-called "Haskind-Newman Relation" in water of finite depth.

3.4 Wave exciting forces and moments by lateral waves

The wave exciting forces and moments of the j-th mode are defined as $E_je^{i\omega t}$, then according to equations (2.8) and (2.14), the forces and the moments normalized by the amplitude of the incident wave are defined as follows:

$$\left.\begin{aligned} e_j&=\frac{E_j}{\rho ga}=-\int_c(\phi_0+\phi_4)\frac{\partial\phi_j}{\partial n}ds,\quad (j=1,2),\\ e_3&=\frac{E_3}{\rho gaT}=-\int_c(\phi_0+\phi_4)\frac{\partial\phi_3}{\partial n}ds. \end{aligned}\right\} \tag{3.20}$$

The velocity potential of incident wave with a unit amplitude is given by

$$\phi_0^{\pm}=\frac{\cosh m_0(h-y)}{\cosh m_0h}e^{\pm im_0x}. \tag{3.21}$$

Since the function ϕ_4 and $\phi_j(j=1,2,3)$ satisfy Laplace's equation, according to Green's theorem, there is a following relation

$$\int_c \phi_4 \frac{\partial \phi_j}{\partial n} ds = \int_c \phi_j \frac{\partial \phi_4}{\partial n} ds, \quad (j=1,2,3). \tag{3.22}$$

And we have $\frac{\partial \phi_4}{\partial n} = -\frac{\partial \phi_0}{\partial n}$ from equation (2.12). Furthermore, substituting these relations into equation (3.20), the following expression can be obtained

$$e_j^{\pm} = -H_j^{\pm}(m_0 h), \quad (j=1,2,3), \tag{3.23}$$

where

$$\left.\begin{aligned} H_j^{\pm}(m_0 h) &= \int_c \left(\frac{\partial \phi_j}{\partial n} - \phi_j \frac{\partial}{\partial n} \right) \frac{\cosh m_0(h-y)}{\cosh m_0 h} e^{\pm m_0 x} ds, \\ H_j^{\pm} &= H_{jc}^{\pm} + iH_{js}^{\pm}, \quad (j=1,2,3). \end{aligned}\right\} \tag{3.24}$$

On the other hand, the velocity potential at infinity can be represented by using of equation (2.16) as follows:

$$\phi_j \underset{x \to \pm\infty}{\sim} iF(m_0 h) \cdot H_j^{\mp}(m_0 h) \cdot \phi_0^{\mp}. \tag{3.25}$$

It is clear from this equation (3.25) that the function H_j^+ is proportional to the amplitude of the wave propagating to the positive direction of x-axis, and that the function H_j^- is similarly proportional to the amplitude of the wave propagating to the negative direction of x-axis. Suppose that the cross section of cylinder is symmetrical, we have

$$|H_j^+(m_0 h)| = |H_j^-(m_0 h)| = H_j(m_0 h), \quad (j=1,2,3).$$

The wave amplitude ratio can be expressed as follows:

$$\hat{A}_j = K \cdot F(m_0 h) \cdot H_j(m_0 h), \quad (j=1,2,3) \tag{3.26}$$

and by equation (3.25) the phase lag ε_j can be written as

$$\varepsilon_j = \tan^{-1}\left(\frac{+H_{jc}}{-H_{js}} \right), \quad (j=1,2,3). \tag{3.27}$$

Substituting the above relations into equation (3.23), the wave exciting forces and moments can be represented by the wave amplitude ratio and the phase lag as follows:

$$e_j = \frac{i\hat{A}_j}{K \cdot F(m_0 h)} e^{i\varepsilon_j}, \quad (j=1,2,3) \tag{3.28}$$

On the other hand, by the natures of the continuity of velocity potential and of the discontinuity of its first order derivative the relation between the function $H_j^{\pm}$ and the source densities distributed on the surface of cylinder can be given as follows:

$$H_j^{\pm}(m_0h)=2\pi\int_c \sigma_j\frac{\cosh m_0(h-y)}{\cosh m_0h}e^{\pm im_0x}ds, \quad (j=1,2,3). \tag{3.29}$$

And from equation (3.6) we have the following relations:

$$\left.\begin{aligned}&\begin{Bmatrix}H_{2c}(m_0h)\\H_{jc}(m_0h)\end{Bmatrix}=2\pi\cdot\begin{Bmatrix}P_{2c}\\-P_{jc}\end{Bmatrix},\\&\begin{Bmatrix}H_{2s}(m_0h)\\H_{js}(m_0h)\end{Bmatrix}=2\pi\cdot\begin{Bmatrix}P_{2s}\\P_{js}\end{Bmatrix},\quad (j=1,3).\end{aligned}\right\} \tag{3.30}$$

Furthermore by eliminating the function H_j from equations (3.17), (3.21) and (3.30), the following equation can be obtained:

$$K^2\cdot F(m_0h)\,|f_{jjs}|=4\pi^2\cdot K^2\cdot F^2(m_0h)\cdot(P_{js}^2+P_{jc}^2),$$

$$\therefore |f_{jjs}|/\{F(m_0h)\cdot(P_{jc}^2+P_{js}^2)\}=4\pi^2, \quad (j=1,2,3). \tag{3.31}$$

This formula is a convenient equation to examine the accuracy of numerical calculations for hydrodynamic forces and moments acting on the cylinder.

3.5 Coefficients of reflective waves and transmissive waves

We extend the relations of water of infinite depth according to [19] to the case of water of finite depth. With aid of Green's theorem by using (2.16) the radiation potential in finite depth of water is represented as

$$\phi_j=\frac{1}{2\pi}\int_c\left(\frac{\partial\phi_j}{\partial n}-\phi_j\frac{\partial}{\partial n}\right)G(x,y;\ x',y')ds, \quad (j=1,2,3). \tag{3.32}$$

Taking into account the symmetrical cross section of cylinder, the radiation potential can be expressed by dividing into a real part and an imaginary part as follows.
In the case of $\phi_2(x,y)=\phi_2(-x,y)$

$$\left.\begin{aligned}\phi_{2c}(x,y)&=\frac{1}{2\pi}\int_c\left(\frac{\partial\phi_{2c}}{\partial n}-\phi_{2c}\frac{\partial}{\partial n}\right)G_c\,ds\\&\quad-F(m_0h)H_{2s}^{+}(m_0h)\frac{\cosh m_0(h-y)}{\cosh m_0h}\cos m_0x,\\\phi_{2s}(x,y)&=\frac{1}{2\pi}\int_c\left(\frac{\partial\phi_{2s}}{\partial n}-\phi_{2s}\frac{\partial}{\partial n}\right)G_c\,ds\\&\quad+F(m_0h)\cdot H_{2c}^{+}(m_0h)\frac{\cosh m_0(h-y)}{\cosh m_0h}\cos m_0x.\end{aligned}\right\} \tag{3.33}$$

In the case of $\phi_j(x,y)=\phi_j(-x,y)$, $(j=1,3)$

$$\left.\begin{aligned}
\phi_{jc}(x,y) &= \frac{1}{2\pi}\int_c\left(\frac{\partial\phi_{jc}}{\partial n}-\phi_{jc}\frac{\partial}{\partial n}\right)G_c\,ds \\
&\quad +iF(m_0h)\cdot H^+_{js}(m_0h)\frac{\cosh m_0(h-y)}{\cosh m_0h}\sin m_0x, \\
\phi_{js}(x,y) &= \frac{1}{2\pi}\int_c\left(\frac{\partial\phi_{js}}{\partial n}-\phi_{js}\frac{\partial}{\partial n}\right)G_c\,ds \\
&\quad -iF(m_0h)\cdot H^+_{jc}(m_0h)\,\frac{\cosh m_0(h-y)}{\cosh m_0h}\sin m_0x.
\end{aligned}\right\}\tag{3.34}$$

Furthermore, from the condition $\frac{\partial\phi_{js}}{\partial n}=0$, $(j=1,2,3)$, and equations (3.33) and (3.34) by taking into account the singularity of the function G_c the condition for an arbitrary point $P(x,y)$ on the surface of cylinder is represented as follows:

$$\left.\begin{aligned}
\frac{1}{2}\phi_{2c}(x,y) &= \frac{1}{2\pi}\int_c\left(\frac{\partial\phi_{2c}}{\partial n}-\phi_{2c}\frac{\partial}{\partial n}\right)G_c\,ds \\
&\quad -F(m_0h)\cdot H^+_{2s}\frac{\cosh m_0(h-y)}{\cosh m_0h}\cos m_0x, \\
\frac{1}{2}\phi_{2s}(x,y) &= \frac{-1}{2\pi}\int_c\phi_{2s}\frac{\partial}{\partial n}G_c\,ds \\
&\quad +F(m_0h)\cdot H^+_{2c}\frac{\cosh m_0(h-y)}{\cosh m_0h}\cos m_0x,
\end{aligned}\right\}\tag{3.35}$$

$$\left.\begin{aligned}
\frac{1}{2}\phi_{jc}(x,y) &= \frac{1}{2\pi}\int_c\left(\frac{\partial\phi_{jc}}{\partial n}-\phi_{jc}\frac{\partial}{\partial n}\right)G_c\,ds \\
&\quad +iF(m_0h)\cdot H^+_{js}\frac{\cosh m_0(h-y)}{\cosh m_0h}\sin m_0x, \\
\frac{1}{2}\phi_{js}(x,y) &= \frac{-1}{2\pi}\int_c\phi_{js}\frac{\partial}{\partial n}G_c ds-iF(m_0h)\cdot H^+_{jc}\cdot\frac{\cosh m_0(h-y)}{\cosh m_0h}\sin m_0x.
\end{aligned}\right\}\tag{3.36}$$

In the next place, since a diffraction potential ϕ_4 is given by

$$\phi_4=\phi_{4A}+i\phi_{4B}$$

where the function ϕ_{4A} and ϕ_{4B} are complex valued functions. From equations (2.12) and (3.21) it follows

$$\left.\begin{aligned}\frac{\partial\phi_{4A}}{\partial n}&=-\frac{\partial}{\partial n}\left\{\frac{\cosh m_0(h-y)}{\cosh m_0h}\cos m_0x\right\},\\ \frac{\partial\phi_{4B}}{\partial n}&=-\frac{\partial}{\partial n}\left\{\frac{\cosh m_0(h-y)}{\cosh m_0h}\sin m_0x\right\}.\end{aligned}\right\}\tag{3.37}$$

The diffraction potential can be written with aid of Green's theorem as

$$\phi_4=\frac{1}{2\pi}\int_c\left(\frac{\partial\phi_4}{\partial n}-\phi_4\frac{\partial}{\partial \mathrm{n}}\right)G\cdot ds=-\frac{1}{2\pi}\int_c\left(\frac{\partial\phi_0}{\partial n}+\phi_4\frac{\partial}{\partial n}\right)Gds,\tag{3.38}$$

and similarly the incident wave potential can be expressed as

$$\phi_0=\frac{1}{2\pi}\int_c\left(\frac{\partial\phi_0}{\partial n}-\phi_0\frac{\partial}{\partial n}\right)G\cdot ds=0.\tag{3.39}$$

Substituting (3. 39) into (3. 38), we have

$$\phi_4=-\frac{1}{2\pi}\int_c(\phi_0+\phi_4)\frac{\partial}{\partial n}G\cdot ds.\tag{3.40}$$

Since it is possible to recognize that the function ϕ_{4A} and ϕ_{4B} are independent each other, the following equations can be obtained:

$$\left.\begin{aligned}\phi_{4A}&=-\frac{1}{2\pi}\int_c\left\{\frac{\cosh m_0(h-y)}{\cosh m_0h}\cos m_0x+\phi_{4A}\right\}\frac{\partial}{\partial n}G\cdot ds,\\ \phi_{4B}&=-\frac{1}{2\pi}\int_c\left\{\frac{\cosh m_0(h-y)}{\cosh m_0h}\sin m_0x+\phi_{4B}\right\}\frac{\partial}{\partial n}G\cdot ds.\end{aligned}\right\}\tag{3.41}$$

And the function $H_4^{\pm}$ can be expressed as

$$\begin{aligned}H_4^{\pm}(m_0h)&=\int_c\left(\frac{\partial\phi_4}{\partial n}-\phi_4\frac{\partial}{\partial n}\right)\frac{\cosh m_0(h-y)}{\cosh m_0h}e^{\pm im_0x}\,ds\\ &=-\int_c(\phi_0+\phi_4)\frac{\partial}{\partial n}\cdot\frac{\cosh m_0(h-y)}{\cosh m_0h}e^{\pm im_0x}\,ds\\ &=H^{\pm}_{4A}+iH^{\pm}_{4B}.\end{aligned}\tag{3.42}$$

Furthermore, since the function $H_4^{\pm}$ has a symmetric relation and an antisymmetric relation, we have the following expressions:

$$\left.\begin{aligned}H^{+}_{4A}(m_0h)&=H^{-}_{4A}(m_0h)=-\int_c(\phi_{0A}+\phi_{4A})\frac{\partial}{\partial n}\cdot\frac{\cosh m_0(h-y)}{\cosh m_0h}\cos m_0x,\\ H^{+}_{4B}(m_0h)&=-H^{-}_{4B}(m_0h)=-i\int_c(\phi_{0B}+\phi_{4B})\frac{\partial}{\partial n}\cdot\frac{\cosh m_0(h-y)}{\cosh m_0h}\sin m_0x.\end{aligned}\right\}\tag{3.43}$$

Now we divide the function ϕ_{4A} and ϕ_{4B} into a real part and an imaginary part as follows:

$$\phi_{4A}=\phi_{4AC}+i\phi_{4AS}, \qquad \phi_{4B}=\phi_{4BC}+i\phi_{4BS}.$$

From the above equations and (3. 37) we have the following expressions:

$$\left.\begin{aligned}
&\frac{\partial}{\partial n}\phi_{4AC}=-\frac{\partial}{\partial n}\phi_{0A}=-\frac{\partial}{\partial n}\cdot\frac{\cosh m_0(h-y)}{\cosh m_0h}\cos m_0x,\\
&\frac{\partial}{\partial n}\phi_{4AS}=0,\\
&\frac{\partial}{\partial n}\phi_{4BC}=-\frac{\partial}{\partial n}\phi_{0B}=-\frac{\partial}{\partial n}\cdot\frac{\cosh m_0(h-y)}{\cosh m_0h}\sin m_0x,\\
&\frac{\partial}{\partial n}\phi_{4BS}=0.
\end{aligned}\right\} \tag{3. 44}$$

According to the above equations and (3. 41), we have the following integral equations satisfying the boundary conditions (2. 12):

$$\left.\begin{aligned}
\frac{1}{2}(\phi_{0A}+\phi_{4AC})=&+\frac{1}{2\pi}\int_c(\phi_{0A}+\phi_{4AC})\frac{\partial}{\partial n}G_c\,ds\\
&+\frac{\cosh m_0(h-y)}{\cosh m_0h}\cos m_0x\{1-F(m_0h)\cdot H^{+}_{4AS}(m_0h)\},\\
\frac{1}{2}\phi_{4AS}=&-\frac{1}{2\pi}\int_c\phi_{4AS}\frac{\partial}{\partial n}G_c ds+F(m_0h)\cdot H^{+}_{4AC}(m_0h)\frac{\cosh m_0(h-y)}{\cosh m_0h}\cos m_0x,
\end{aligned}\right\} \tag{3. 45}$$

$$\left.\begin{aligned}
\frac{1}{2}(\phi_{0B}+\phi_{4BC})=&-\frac{1}{2\pi}\int_c(\phi_{0B}+\phi_{4BC})\frac{\partial}{\partial n}G_c\,ds\\
&+\frac{\cosh m_0(h-y)}{\cosh m_0h}\sin m_0x\{1+iF(m_0h)\cdot H^{+}_{4BS}(m_0h)\},\\
\frac{1}{2}\phi_{4BS}=&-\frac{1}{2\pi}\int_c\phi_{4BS}\frac{\partial}{\partial n}G_c ds-iF(m_0h)\cdot H^{+}_{4BC}(m_0h)\frac{\cosh m_0(h-y)}{\cosh m_0h}\sin m_0x.
\end{aligned}\right\} \tag{3. 46}$$

Since these equations (3. 35), (3. 36), (3. 45) and (3. 46) are the second kind of the integral equations of Fredholm Type, it is able to recognize that these equations have solutions respectively and the dependent relations among these solutions can be obtained as follows:

$$\frac{H^{+}_{2S}(m_0h)}{H^{+}_{2C}(m_0h)}=\frac{H^{+}_{4AS}(m_0h)}{H^{+}_{4AC}(m_0h)}, \tag{3. 47}$$

$$\frac{H_{jS}^{+}(m_0h)}{H_{jC}^{+}(m_0h)}=\frac{H_{4BS}^{+}(m_0h)}{H_{4BC}^{+}(m_0h)}.\ (j=1,3) \tag{3.48}$$

similarly

$$(\phi_{0A}+\phi_{4AC})\cdot F(m_0h)\cdot H_{4AC}^{+}=\phi_{4AS}\{1-F(m_0h)\cdot H_{4AS}^{+}\},$$

$$(\phi_{0B}+\phi_{4BC})\cdot F(m_0h)\cdot H_{4BC}^{+}=i\phi_{4BS}\{1+iF(m_0h)\cdot H_{4BS}^{+}\}.$$

From the above equations and (3.43) the following equations can be obtained as

$$\left.\begin{aligned} H_{4AS}^{+}&=F(m_0h)\{(H_{4AC}^{+})^2+(H_{4AS}^{+})^2\},\\ iH_{4AS}^{+}&=F(m_0h)\{(H_{4BC}^{+})^2+(H_{4BS}^{+})^2\}.\end{aligned}\right\} \tag{3.49}$$

By putting on

$$\frac{H_{1S}^{+}}{H_{1C}^{+}}=\tan\alpha_1,\qquad \frac{H_{2S}^{+}}{H_{2C}^{+}}=\tan\alpha_2, \tag{3.50}$$

from (3.47) and (3.48) the function $H_4^{\pm}$ can be represented as

$$H_4^{\pm}=\frac{1}{F(m_0h)}(\mathrm{e}^{i\alpha_2}\sin\alpha_2\mp\mathrm{e}^{i\alpha_1}\sin\alpha_1). \tag{3.51}$$

Concidering that the functions H_{1C}^{+} and H_{1S}^{+} are imaginary and the functions H_{2C}^{+} and H_{2S}^{+} are real, we have

$$\alpha_1=\varepsilon_1-\pi,\qquad \alpha_2=\varepsilon_2-\frac{\pi}{2}. \tag{3.52}$$

The function $H_4^{\pm}$ can be rewritten according to the above relations as follows:

$$H_4^{\pm}=\frac{1}{F(m_0h)}(i\mathrm{e}^{i\varepsilon_2}\cos\varepsilon_2\mp\mathrm{e}^{i\varepsilon_1}\sin\varepsilon_1). \tag{3.53}$$

The outgoing wave amplitude at infinity, according to the diffractin potential ϕ_4, are given as

$$\hat{\eta}_{x\to\pm\infty}\sim iH_4^{\pm}\cdot F(m_0h)\frac{\cosh m_0(h-y)}{\cosh m_0h}\mathrm{e}^{\mp im_0x}. \tag{3.54}$$

When the incident wave with an unit amplitude incomes to a rigid body from a possitive direction of x-coordinate axis, the wave amplitude at infinity, $x\to\pm\infty$, can be expressed as follows:

$$\left.\begin{aligned}\hat{\eta}_{+\infty} &\sim iH_4^{+}\cdot F(m_0h)\frac{\cosh m_0(h-y)}{\cosh m_0h}e^{-im_0x},\\ \hat{\eta}_{-\infty} &\sim \{1+iH_4^{-}\cdot F(m_0h)\}\frac{\cosh m_0(h-y)}{\cosh m_0h}e^{+im_0x}.\end{aligned}\right\} \tag{3.55}$$

When there is a rigid body in water of finite depth, the coefficients of reflective wave and transmissive wave can be consequently expressed as follows:

$$C_R=|iH_4^{+}(m_0h)\cdot F(m_0h)|, \tag{3.56}$$

$$C_T=|1+iH_4^{-}(m_0h)\cdot F(m_0h)|. \tag{3.57}$$

4. Comparison experimental results with numerical results for two dimensional hydrodynamic forces and moments

4.1 Numerical method to find Green's function and stream function

Since it is very difficult to solve analytically the integral equations in the previous sections, we suppose that the source densities on the cross section, where the surface of cylinder are divided into N-parts, are constant respectively, and solve two system of linear equations with $(N+1)$-unknown variables which are unknown source densities σ_{jc} and σ_{js} and integral constants C_{jc} and C_{js} $(j=1,2,3)$. Thus the distribution of source densities can be evaluated by the above method.

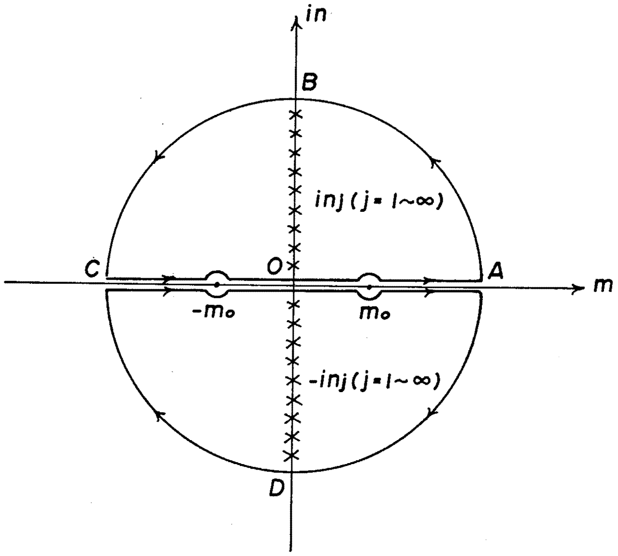

Fig. 4.1 Line of integration in the complex plane

In this case the numerical method to find Green's function and stream function are as follows.

The term of logarithms in (2. 16) is transformed to the expression of infinite integral [22] and the principal value integral taking the line of integration in complex plane shown in Fig. 4. 1 is carried out and is transformed to the infinite series given by

$$G_c = \frac{4\pi \cosh m_0(h-y) \cosh m_0(h-y')}{2m_0h+\sinh 2m_0h} \sin m_0|x-x'| - 4\pi \sum_{j=1}^{\infty} \frac{\cos n_j(h-y) \cos n_j(h-y')}{2n_jh+\sin 2n_jh} e^{-n_j|x-x'|}. \tag{4. 1}$$

In the next place, as for the stream function corresponding to the above Green's function we consider similarly the following two domains, we have

$$S_c = -\operatorname{sgn}(x-x') \left\{ \frac{4\pi \sinh m_0(h-y) \cosh m_0(h-y')}{2m_0h+\sinh 2m_0h} \cos m_0(x-x') + 4\pi \sum_{j=1}^{\infty} \frac{\sin n_j(h-y) \cos n_j(h-y')}{2n_jh+\sin 2n_jh} e^{-n_j|x-x'|} \right\} - 2\pi, \tag{4. 2}$$

for $x-x'<0, \quad y-y'<0,$

and

$$S_c = -\operatorname{sgn}(x-x') \left\{ \frac{4\pi \sinh m_0(h-y) \cosh m_0(h-y')}{2m_0h+\sinh 2m_0h} \cos m_0(x-x') + 4\pi \sum_{j=1}^{\infty} \frac{\sin n_j(h-y) \cos n_j(h-y')}{2n_jh+\sin 2n_jh} e^{-n_j|x-x'|} \right\}, \tag{4. 3}$$

except for the above one.

It is necessary to calculate the infinite series G_c and S_c. Now putting the errors of the sum with N-terms in infinite series GER, SER respectively, the functions GER and SER are represented [23] as

$$GER = \frac{\left| -\frac{1}{8\pi} \log(1-2e^{-\gamma}\cos\alpha+e^{-2\gamma})(1-2e^{-\gamma}\cos\beta+e^{-2\gamma}) - \frac{1}{2\pi}\sum_{j=1}^{N} \frac{\cos j\left(\frac{\alpha+\beta}{2}\right)\cos j\left(\frac{\alpha-\beta}{2}\right)}{j} e^{-j\gamma} \right|}{\left| \sum_{j=1}^{N} \frac{\cos n_j(h-y) \cos n_j(h-y')}{2n_jh+\sin 2n_jh} e^{-n_j|x-x'|} \right|}, \tag{4. 4}$$

$$SER=\frac{\left| -\frac{1}{4\pi}\left(\tan^{-1}\frac{e^{-\gamma}\sin\alpha}{1-e^{-\gamma}\cos\alpha}+\tan^{-1}\frac{e^{-\gamma}\sin\beta}{1-e^{-\gamma}\cos\beta}\right) + \frac{1}{2\pi}\sum_{j=1}^{N}\frac{\sin j\left(\frac{\alpha+\beta}{2}\right)\cos j\left(\frac{\alpha-\beta}{2}\right)}{j}e^{-j\gamma} \right|}{\left|\sum_{j=1}^{N}\frac{\sin n_j(h-y)\cos n_j(h-y')}{2n_jh+\sin 2n_jh}e^{-n_j|x-x'|}\right|},$$

$$\text{where}\quad \alpha=\frac{\pi}{h}(y+y'),\quad \beta=\frac{\pi}{h}(y-y'),\quad \gamma=\frac{\pi}{h}|x-x'|. \tag{4.5}$$

The errors GER and SER for instance $|x-x'|/\frac{B}{2}=0.2$, $KT=0.5$ are shown in Table 4-1. According to this table it is obvious that the errors GER and SER become large as the depths of water become deep. In order to calculate the values of the Green's function and the stream function within *0.1%* with maximum error, we calculate those taking the number of terms $N=20$ in infinite series.

Table 4-1 Errors of infinite series ($|x-x'|/\frac{B}{2}=0.2$, $KT=0.5$)

N	ERR \ h/T	1.1	1.5	2.0	4.0	6.0
10	GER SER	0.88×10^{-4} 0.76×10^{-3}	0.24×10^{-2} 0.28×10^{-2}	0.54×10^{-2} 0.59×10^{-1}	0.76×10^{-2} 0.95×10^{-1}	0.63×10^{-1} 0.30×10^{-1}
20	GER SER	0.29×10^{-5} 0.14×10^{-5}	0.10×10^{-4} 0.28×10^{-4}	0.19×10^{-3} 0.85×10^{-4}	0.62×10^{-3} 0.27×10^{-2}	0.45×10^{-2} 0.97×10^{-2}
30	GER SER	0.35×10^{-5} 0.21×10^{-5}	0.27×10^{-5} 0.44×10^{-5}	0.33×10^{-5} 0.56×10^{-4}	0.88×10^{-3} 0.10×10^{-2}	0.12×10^{-2} 0.21×10^{-2}
50	GER SER	0.35×10^{-5} 0.21×10^{-5}	0.30×10^{-5} 0.56×10^{-5}	0.95×10^{-5} 0.15×10^{-4}	0.33×10^{-4} 0.70×10^{-5}	0.21×10^{-3} 0.72×10^{-4}
100	GER SER	0.35×10^{-5} 0.21×10^{-5}	0.30×10^{-5} 0.56×10^{-5}	0.95×10^{-4} 0.15×10^{-4}	0.87×10^{-6} 0.20×10^{-6}	0.68×10^{-4} 0.17×10^{-5}

In the next place, the error of GER and SER become large because of a slow convergence if the number of terms N are not taken to sum up much more in the case $|x-x'|/\frac{B}{2}<0.2$. And so we transform the equations (2.16) and (2.17) to the following forms in order to reduce the computing time. The velocity potential is written by

$$G(x,y;\ x',y')=G_c(x,y;\ x',y')+iG_s(x,y;\ x',y')$$

$$=\log\frac{r_1}{r_2}+2\cdot\text{P.V.}\int_0^\infty\frac{e^{-k(y+y')}}{K-k}\cos k(x-x')dk$$

$$+2\cdot\mathrm{P.V.}\int_0^\infty \frac{e^{-kh}(K\sinh ky'-k\cosh ky')\ (k\cosh ky-K\sinh ky)}{k(K-k)(K\cosh kh-k\sinh kh)}$$

$$\times\cos k(x-x')dk$$

$$+i\frac{4\pi\cosh m_0(h-y)\ \cosh m_0(h-y')}{2m_0h+\sinh 2m_0h}\cos m_0(x-x')$$

$$=\log\frac{r_1}{r_2}+I_\infty+I_h+iG_s \tag{4.6}$$

$$\left.\begin{array}{l}\lim\limits_{h\to\infty} I_h\to 0,\\ \lim\limits_{h\to\infty} G_s\to 2\pi e^{-K(y+y')}\cos K(x-x').\end{array}\right\} \tag{4.7}$$

The stream function is represented by

$$S(x,y;\ x',y')=S_c(x,y;\ x',y')+iS_s(x,y;\ x',y')$$

$$=\theta_1-\theta_2+2\cdot\mathrm{P.V.}\int_0^\infty\frac{e^{-k(y+y')}}{K-k}\sin k(x-x')dk$$

$$+2\cdot\mathrm{P.V.}\int_0^\infty \frac{e^{-kh}(K\sinh ky'-k\cosh ky')(K\cosh ky-k\sinh ky)}{k(K-k)(K\cosh kh-k\sinh kh)}$$

$$\times\sin k(x-x')dk$$

$$+i\frac{4\pi\sinh m_0(h-y)\ \cosh m_0(h-y')}{2m_0h+\sinh 2m_0h}\sin m_0(x-x')$$

$$=(\theta_1-\theta_2)+J_\infty+J_h+iS_s. \tag{4.8}$$

$$\left.\begin{array}{l}\lim\limits_{h\to\infty} J_h\to 0,\\ \lim\limits_{h\to\infty} S_s\to 2\pi\ e^{-K(y+y')}\sin K(x-x').\end{array}\right\} \tag{4.9}$$

The third terms I_h in (4.6) and J_h in (4.8) become to zero as the depths of water become infinitely deep, and the function $G(x,y;\ x',y')$ and $S(x,y;\ x',y')$ coincide with the Green's function and the stream function in the case of infinitely deep water respectively. Namely by adding the third terms I_h and J_h to the equations of infinitely deep water, these equations satisfy the conditions of water of finite depth. Making a computer program of equations (4.6) and (4.8), the computer program to calculate the hydrodynamic forces in water of finite depth is completed and at the same time the computer program in the case of water of infinite depth is completed. On the other hand, if we have a computer program to calculate the hydrodynamic forces of infinitely deep water by the so-called "close fit method", we can make easily a computer program to calculate the hydrodynamic forces in water of finite depth by adding the third terms I_h and J_h to the eqations in water of infinite depth. Therefore these (4.6) and (4.8) are very convenient equations.

The calculating methods of the first term and the second term of (4.6) and (4.8) in water of infinite depth have been studied by many researchers[21), 24)], we omit the calculating methods of those and deal with the method of calculation of the third terms I_h and J_h in each equation. We use the following notations in Fig. 2.1.

$$\left.\begin{aligned}&V=Kh, \quad u=kh, \quad \beta_1=\tan^{-1}\frac{x}{y}, \quad \beta_2=\tan^{-1}\frac{x'}{y'},\\ &y_{h1}=y/h, \quad y_{h2}=y'/h, \quad x_{h1}=x/h, \quad x_{h2}=x'/h,\\ &r_{h1}=(x^2+y^2)^{1/2}/h, \quad r_{h2}=(x'^2+y'^2)^{1/2}/h.\end{aligned}\right\} \tag{4.10}$$

The third terms I_h and J_h are transformed to the following double series which involve the singular integrals $F_{2s+1}(V)$, $F_{2s+3}(V)$ respectively.

$$\begin{aligned}I_h = \sum_{s=0}^{\infty} F_{2s+1}(V)\Bigg\{&-V^2\sum_{t=0}^{s}\frac{r_{h1}{}^{2s-2t+1}\cdot r_{h2}{}^{2t+1}\cos(2s-2t+1)\beta_1\cdot\cos(2t+1)\beta_2}{(2s-2t+1)!\,(2t+1)!}\\ &+V\sum_{t=0}^{s}\frac{r_{h2}{}^{2s-2t+1}\cdot r_{h2}{}^{2t}\cos(2s-2t+1)\beta_1\cdot\cos 2t\beta_2}{(2s-2t+1)!\,(2t)!}\\ &+V\sum_{t=0}^{s}\frac{r_{h1}{}^{2t}\cdot r_{h2}{}^{2s-2t+1}\cdot\cos 2t\beta_1\cdot\cos(2s-2t+1)\beta_2}{(2s-2t+1)!\,(2t)!}\\ &-\sum_{t=0}^{s}\frac{r_{h1}{}^{2s-2t}\cdot r_{h2}{}^{2t}\cdot\cos(2s-2t)\beta_1\cdot\cos 2t\beta_2}{(2s-2t)!\,(2t)!}\Bigg\}\\ +\sum_{s=0}^{\infty} F_{2s+3}(V)\Bigg\{&-V^2\sum_{t=0}^{s}\frac{r_{h1}{}^{2s-2t+2}\cdot r_{h2}{}^{2t+2}\cdot\sin(2s-2t+2)\beta_1\cdot\sin(2t+2)\beta_2}{(2s-2t+2)!\,(2t+2)!}\\ &+V\sum_{t=0}^{s}\frac{r_{h1}{}^{2s-2t+2}\cdot r_{h2}{}^{2t+1}\cdot\sin(2s-2t+2)\beta_1\cdot\sin(2t+1)\beta_2}{(2s-2t+2)!\,(2t+1)!}\\ &+V\sum_{t=0}^{s}\frac{r_{h1}{}^{2t+1}\cdot r_{h2}{}^{2s-2t+2}\cdot\sin(2t+1)\beta_1\cdot\sin(2s-2t+2)\beta_2}{(2s-2t+2)!\,(2t+1)!}\\ &-\sum_{t=0}^{s}\frac{r_{h1}{}^{2s-2t+1}\cdot r_{h2}{}^{2t+1}\cdot\sin(2s-2t+1)\beta_1\cdot\sin(2t+1)\beta_2}{(2s-2t+1)!\,(2t+1)!}\Bigg\},\end{aligned} \tag{4.11}$$

$$\begin{aligned}J_h = \sum_{s=0}^{\infty} F_{2s+1}(V)\Bigg\{&V^2\sum_{t=3}^{s}\frac{r_{h1}{}^{2s-2t+1}\cdot r_{h2}{}^{2t+1}\cdot\sin(2s-2t+1)\beta_1\cdot\cos(2t+1)\beta_2}{(2s-2t+1)!\,(2t+1)!}\\ &-V^2\sum_{t=0}^{s}\frac{r_{h1}{}^{2t}\cdot r_{h2}{}^{2s-2t+2}\cdot\cos 2t\beta_1\cdot\sin(2s-2t+2)\beta_2}{(2s-2t+2)!\,(2t)!}\\ &-V\sum_{t=0}^{s}\frac{r_{h1}{}^{2s-2t+1}\cdot r_{h2}{}^{2t}\cdot\sin(2s-2t+1)\beta_1\cdot\cos 2t\beta_2}{(2s-2t+1)!\,(2t)!}\end{aligned}$$

$$+V\sum_{t=0}^{s}\frac{r_{h1}^{\ 2t}\cdot r_{h2}^{\ 2s-2t+1}\cdot\cos 2t\beta_1\cdot\sin(2s-2t+1)\beta_2}{(2s-2t+1)!\ (2t)!}$$

$$+\sum_{s=0}^{\infty}F_{2s+3}(V)\left\{V\sum_{t=0}^{s}\frac{r_{h1}^{\ 2t+1}\cdot r_{h2}^{\ 2s-2t+2}\cdot\cos(2t+1)\beta_1\cdot\sin(2s-2t+2)\beta_2}{(2s-2t+2)!\ (2t+1)!}\right.$$

$$-V\sum_{t=0}^{s}\frac{r_{h1}^{\ 2s-2t+2}\cdot r_{h2}^{\ 2t+1}\cdot\sin(2s+2t+2)\beta_1\cdot\cos(2t+1)\beta_2}{(2s-2t+2)!\ (2t+1)!}$$

$$+\sum_{t=0}^{s}\frac{r_{h1}^{\ 2s-2t+2}\cdot r_{h2}^{\ 2t}\cdot\sin(2s-2t+2)\beta_1\cdot\cos 2t\beta_2}{(2s-2t+2)!\ (2t)!}$$

$$\left.-\sum_{t=0}^{s}\frac{r_{h1}^{\ 2t+1}\cdot r_{h2}^{\ 2s-2t+1}\cdot\cos(2t+1)\beta_1\cdot\sin(2s-2t+1)\beta_2}{(2s-2t+1)!\ (2t+1)!}\right\}. \tag{4.12}$$

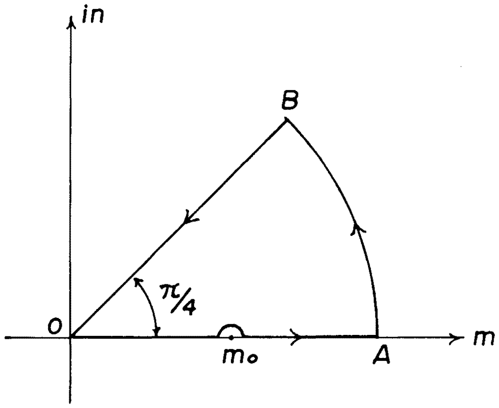

Fig. 4.2 Line of integration in the complex plane

where the singular integrals $F_{2s+1}(V), F_{2s+3}(V)$ involving the non-dimensional frequency parameter V only can be represented by taking the line of integration in the complex plane shown in Fig. 4.2 as follows [25]:

$$F_{2s+1}(V)=\text{P. V.}\int_0^{\infty}\frac{e^{-u}\cdot u^{2s+1}\cdot du}{(V-u)\ (V\cosh u-u\sinh u)}=\int_0^{\infty}\frac{N_{2s+1}}{D_{2s+1}}db. \tag{4.13}$$

$$N_{2s+1}=-\frac{b^{2s+1}}{2^{s+2}}\left[V^2\left\{e^{-b}\sin\frac{s\pi}{2}+\sin\left(\frac{s\pi}{2}-b\right)\right\}\right.$$

$$+bV\left\{\cos\left(\frac{s\pi}{2}-b\right)-\sin\left(\frac{s\pi}{2}-b\right)\right\}$$

$$+\frac{b^2}{2}\left\{e^{-b}\cos\frac{s\pi}{2}-\cos\left(\frac{s\pi}{2}-\mathrm{b}\right)\right\}\Big]. \tag{4.14}$$

$$D_{2s+1}=\frac{1}{2}\left(V^2-bV+\frac{b^2}{2}\right)\Big\{V^2(\cosh b+\cos b)-bV(\sinh b-\sin b)$$

$$+\frac{b^2}{2}(\cosh b-\cos b)\Big\}. \tag{4.15}$$

$$F_{2s+3}(V)=\mathrm{P.V.}\int_0^\infty\frac{e^{-u}\cdot u^{2s+3}\,du}{(V-u)(V\cosh u-u\sinh u)}=\int_0^\infty\frac{N_{2s+3}}{D_{2s+3}}db. \tag{4.16}$$

$$N_{2s+3}=-\frac{b^{2s+3}}{2^{s+3}}\Big[V^2\left\{e^{-b}\cos\frac{s\pi}{2}+\cos\left(\frac{s\pi}{2}-b\right)\right\}$$

$$-bV\left\{\cos\left(\frac{s\pi}{2}-b\right)+\sin\left(\frac{s\pi}{2}-b\right)\right\}$$

$$-\frac{b^2}{2}\left\{e^{-b}\sin\frac{s\pi}{2}-\sin\left(\frac{s\pi}{2}-b\right)\right\}\Big]. \tag{4.17}$$

$$D_{2s+3}=D_{2s+1}. \tag{4.18}$$

In the numerical calculating equations (4.13) and (4.16) with aid of Simpson's rule, it is necessary to determine the mesh size of Simpson's rule, because the behavior of $F_{2s+1}(V)$ for the mesh size $b=0.02$, 0.05, 0.1 and 0.5 are shown in Fig. 4.3 as the functions of frequency V and it is seen that the effect of mesh size of Simpson's rule depends on the accuracy of the singular function $F_{2s+1}(V)$ in low frequency range and it leads to the wrong calculated results consequently.

Table 4-2 Mesh size b for Simpson's rule

	Frequency $(V=\frac{\omega^2}{g}h)$	Mesh size (b)
$S=0$	$0 \leq V \leq 0.015$	$b=0.001$
	$0.015 < V \leq 0.04$	$b=0.01$
	$0.04 < V \leq 0.10$	$b=0.02$
	$0.10 < V\ \ 0.20$	$b=0.05$
	$0.20 < V \leq 1.0$	$b=0.10$
	$1.0 < V < \infty$	$b=0.50$
$S=1$	$0 \leq V \leq 1.0$	$b=0.10$
	$1.0 < V < \infty$	$b=0.50$
$S=2$	$0 < V \leq 0.2$	$b=0.10$
	$0.2 < V < \infty$	$b=0.50$
$S=3$	$0 \leq V < \infty$	$b=0.50$

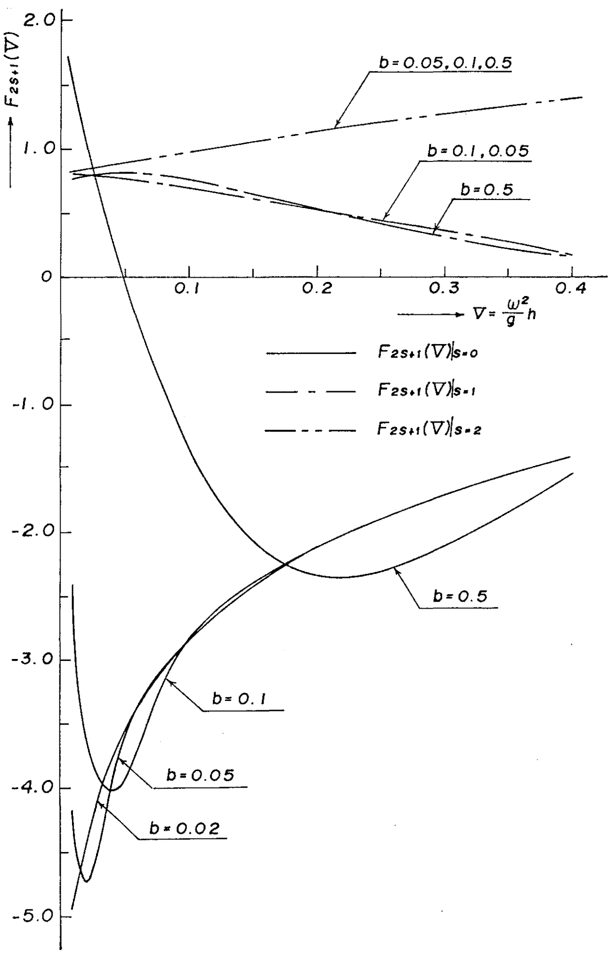

Fig. 4.3 Behavior of the singular function $F_{2S+1}(V)$ for varying b at low frequency

C. H. Kim also has recently corrected his numerical results by taking into account this effect [26]. The mesh size b used in our calculations are shown in Table 4-2. And the limits of integrations by using Simpson's rule are determined within *0.1%* with maximum error. The number of suffix S in double series I_h and J_k are taken from $S=0$ to 7 because the numerical results obtained by taking $S=7$ coincides with the ones obtained by $S=8$ up to five significant figures.

4.2 Accuracy of the numerical calculations

The accuracies of numerical calculations become good as the numbers of dividing the surface of cylinder become much. The accuracies of the numerical calculations of the hydrodynamic forces for heaving semi-circular cylinder with the valuable dividing number of surface of one side $N=4$, 8, 12, 16, 20, 30 and 40 are shown in Table 4-3. It is obvious that the accuracies of numerical results become good as the dividing numbers become much and the depth of water does not depend on the accuracies of numerical results too much and the hydrodynamic forces of very shallow water $h/T=1.1$ also can be obtained with a good accuracy due to this table. Since the maximum error for calculating with $N=20$ is no more than 0.2% at the most, we think the accuracies of results obtained with $N=20$ to be enough and have calculated with the dividing number $N=20$ hereafter.

Sayer and Ursell have recently calculated the added mass of heaving semi-circular cylinder in water of finite depth at the low frequency $KT=0$.[3)]

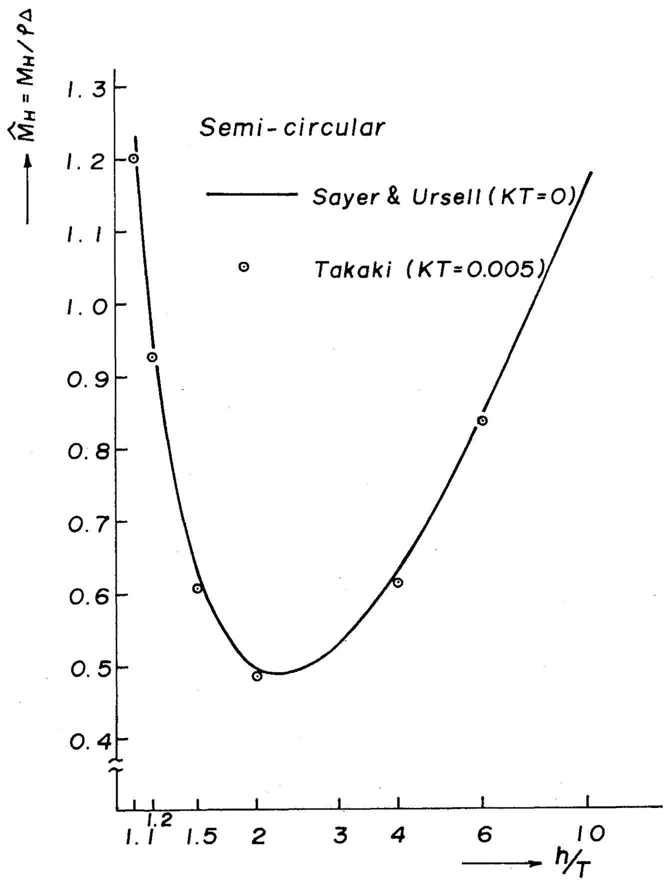

Fig. 4.4 $\hat{M}_H$: Added mass coeff. of heave for semi-circular

Table 4-3 Accuracies of hydrodynamic forces for heaving semi-circular cylinder

N	h/T \ KT	1.1	1.2	1.5	2.0	4.0	6.0	10.0
4	0.50 1.00	1.0208 1.0152	1.0036 0.99488	0.99770 0.98890	0.99758 0.98907	0.99755 0.9828	0.99720 0.98760	1.0026 0.99361
8	0.50 1.00	0.99966 0.99755	0.99952 0.99754	0.99975 0.99829	0.99987 0.99874	1.C001 0.99891	0.99992 0.99798	1.0036 1.0072
12	0.50 1.00	1.0001 0.99980	1.0000 0.99958	1.0001 0.99989	1.0002 1.0002	1.0002 1.0002	0.99910 0.99878	0.99883 1.0017
16	0.50 1.00	1.0002 1.0006	1.0001 1.0002	1.0002 1.0003	1.0002 1.0005	1.0003 1.0008	1.0003 1.0011	1.0004 1.0011
20	0.50 1.00	1.0003 1.0008	1.0002 1.0004	1.0002 1.0004	1.0002 1.0006	1.0002 1.0006	1.0011 1.0028	1.0004 0.99806
30	0.50 1.00	1.0001 1.0007	1.0001 1.0005	1.0002 1.0004	1.0001 1.0005	1.0000 1.0002	1.0003 1.C013	0.99748 0.99597
40	0.50 1.00	1.0003 1.0011	1.0002 1.0005	1.0001 1.0004	1.0001 1.0005	1.0002 1.0004	1.0008 1.0008	1.0012 1.0015

Their results and our results (our results are not $KT=0$ but $KT=0.005$) are shown in Fig. 4.4. It is seen from this figure that we obtained good numerical results at such a very low frequency range by this calculated method.

4.3 Analysis of forced oscillation test

The forced oscillation test was performed in the small experimental tank ($L\times B\times D=60$ m$\times$1.5 m$\times$1.5 m) of the Tsuyazaki Sea Safety Research Laboratory belonging to the Research Institute for Applied Mechanics of Kyushu University. Photo 4-1 shows the condition of forced heaving test and Photo 4-2 shows the condition of laterally forced oscillation test. Three model ships used in this experiment have the two dimensional Lewis form cross section shown in Fig. 4.5, and the lengths of models are all 1.45 m in order to keep the two-dimensional test condition. The forced heaving test and the laterally forced oscillation test (swaying and rolling) were carried out in the different test conditions respectively. Namely, the forced heaving test was performed in four kinds of water depth ($h=130.0$ cm, 59.2 cm, 31.4 cm and 21.5 cm) by using only the model with a rectangular cross section. On the other hand, the laterally forced oscillation tests were carried out in various depths of water ($h=124.5$ cm, 66.5 cm, 32 cm, and 22.5 cm) by using three ship models shown in Fig. 4.5. In these experiments the test of the rectangular model was carried out with a bilge-keel of 10 mm breadth and the tests of semi-circular model were carried out with and without a bilge-keel.

We measured the displacements of the cylinders, the hydrodynamic forces and moments acting on the ship models and the amplitude of outgoing waves.

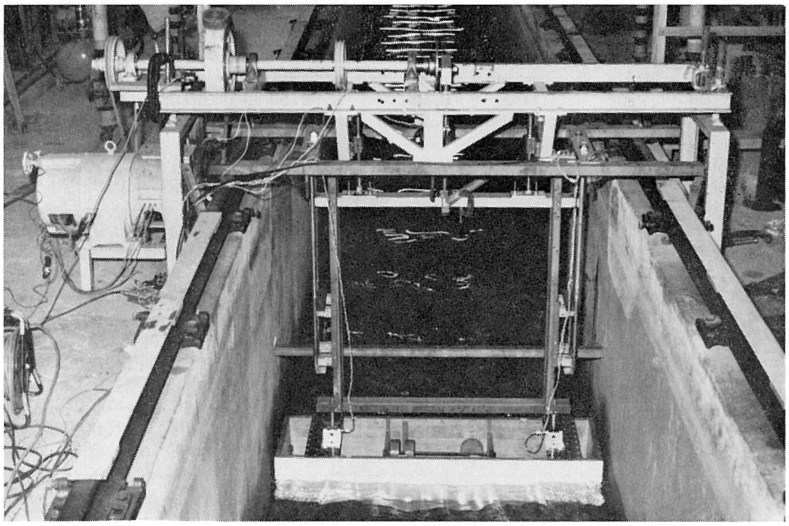

Photo 4-1 Condition of forced heaving test

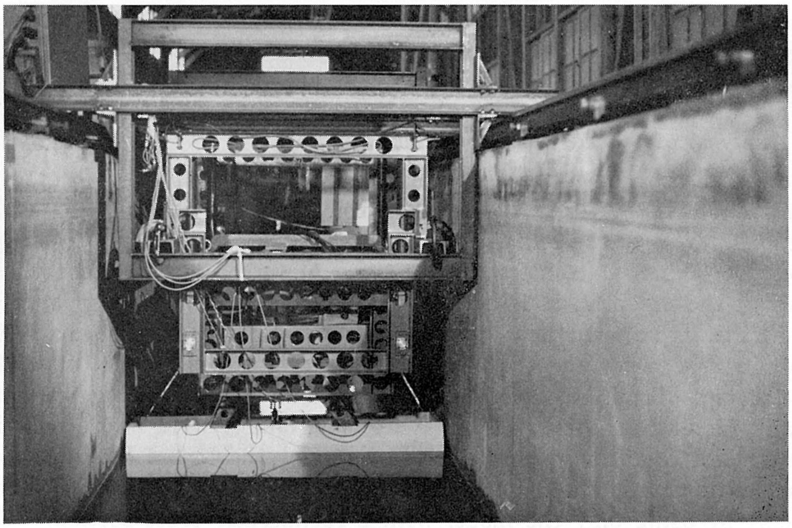

Photo 4-2 Condition of laterally forced oscillation test

The swaying force, the rolling moment and the coupling force acting on the ship model were composed with three forces which were measured by the three strain-gauge dynamometers [27]. The amplitude of the outgoing waves was measured by the wave height meter which was set at the point from the ship model by 5m. Thus the forces and the wave height measured

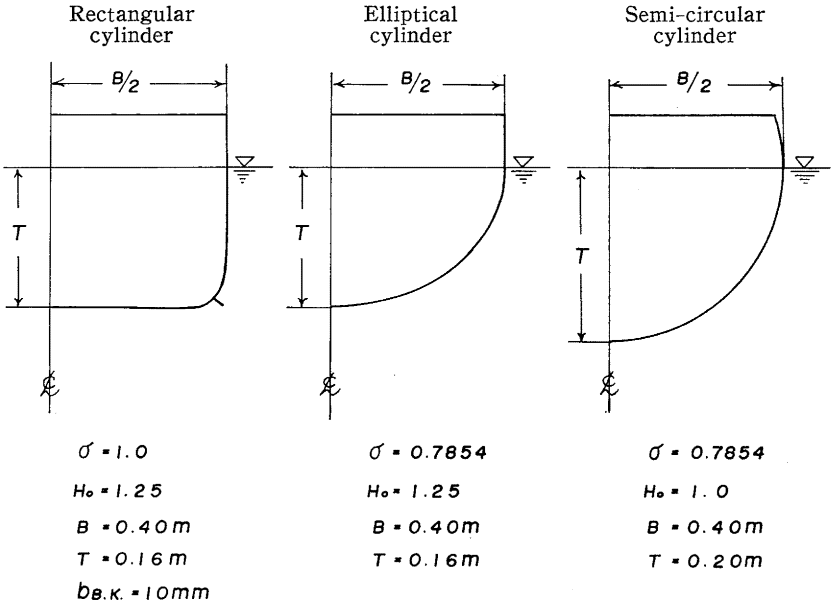

Fig. 4.5 Cross sectional forms of models

were analyzed with aid of Fourier expansion, and we compared the numerical results with the experimental results of the first order with the circular frequency ω.

Now, the heaving equation and the coupling equations between swaying and rolling about O (shown in Fig. 2.1) are represented as follows:

$$(\rho\varDelta+M_H)\ddot{\zeta}+N_H\,\dot{\zeta}+\rho g A_W\,\zeta=Z_A\,\sin(\omega t+\varepsilon_Z), \tag{4.19}$$

$$\begin{cases}(\rho\varDelta+M_S)\ddot{\eta}+N_S\dot{\eta}+(M_{\phi\eta}-\rho\varDelta\,\overline{OG})\ddot{\phi}+N_{\phi\eta}\dot{\phi}=Y_A\,\sin(\omega t+\varepsilon_Y),\\(J_\phi+M_R)\ddot{\phi}+N_R\dot{\phi}+\rho g\varDelta\cdot\overline{GM}\phi+(M_{\eta\phi}-\rho\varDelta\,\overline{OG})\ddot{\eta}+N_{\eta\phi}\dot{\eta}=L_A\,\sin(\omega t+\varepsilon_L),\end{cases} \tag{4.20}$$

where the direction of moment is crockwise,

$$M_{\eta\phi}=M_{\phi\eta}=-\rho\varDelta\cdot l_{SR}, \qquad N_{\eta\phi}=N_{\phi\eta}=-N_s\cdot l_\omega,$$

Z_A: Heaving exciting force, ε_Z: Phase lag between heaving displacement and heaving hydrodynamic force,
Y_A: Swaying exciting force, ε_Y: Phase lag between swaying displacement and swaying hydrodynamic force,
L_A: Rolling exciting moment, ε_L: Phase lag between rolling displacement and rolling hydrodynamic moment.

(i) The forced heaving test

The origin of two-dimensional model ship O is forced to a harmonic oscillation $\zeta = Z_A \sin \omega t$. Then the coefficients of hydrodynamic forces with the first order of circular frequency ω can be obtained from equation (4.19) as follows:

$$\left.\begin{aligned} M_H &= -\frac{Z_A \cos \varepsilon_Z}{\omega^2 z_A} - \rho\Delta + \frac{\rho g A_W}{\omega^2}: \text{ Addedmass of heave} \\ N_H &= \frac{Z_A \sin \varepsilon_Z}{\omega z_A}: \text{ Damping force of heave,} \end{aligned}\right\} \tag{4.21}$$

$Z_A = 1.5$ cm: Heaving amplitude.

(ii) The forced swaying test

The origin of two-dimensional cylinder O is forced to a harmonic oscillation $\eta = y_A \sin \omega t$. Then it means that $\ddot{\phi} = \dot{\phi} = 0$ and the relations between the coefficients of hydrodynamic forces and moments with the first order of circular frequency ω can be oatained from equation (4.20) as follows.

$$\left.\begin{aligned} M_S &= -\frac{Y_A \cos \varepsilon_Y}{\omega^2 y_A} - \rho\Delta: \quad \text{Addedmass of sway,} \\ N_S &= \frac{Y_A \sin \varepsilon_Y}{\omega y_A}: \quad \text{Damping force of sway,} \end{aligned}\right\} \tag{4.22}$$

$$\left.\begin{aligned} M_{\eta\phi} &= -\frac{L_A \cos \varepsilon_L}{\omega^2 y_A} + \rho\Delta \cdot \overline{OG} \\ N_{\eta\phi} &= \frac{L_A \sin \varepsilon_L}{\omega y_A} \end{aligned}\right\} \text{ Coupling moment of sway into roll.} \tag{4.23}$$

$y_A = 2$ cm: Swaying amplitude.

(iii) Forced rolling test

The two-dimensional ship model is forced to a harmonic oscillation $\phi = \phi_A \sin \omega t$ about the point O origin of ship model. Then it means that $\ddot{\eta} = \dot{\eta} = 0$ and the coefficients of equation (4.20) have the following relations.

$$\left.\begin{aligned} J_\phi + M_R &= -\frac{L_A \cos \varepsilon_L}{\omega^2 \phi_A} + \frac{\rho g \Delta \cdot GM}{\omega^2}: \text{ Virtual mass moment of inertia of roll,} \\ N_R &= \frac{L_A \sin \varepsilon_L}{\omega \phi_A}: \text{ Damping moment coeff. of roll,} \end{aligned}\right\} \tag{4.24}$$

$$\left.\begin{aligned} M_{\phi\eta} &= -\frac{Y_A \cos \varepsilon_Y}{\omega^2 \phi_A} + \rho\Delta\overline{OG} \\ N_{\phi\eta} &= \frac{Y_A \sin \varepsilon_Y}{\omega \phi_A} \end{aligned}\right\} \text{ Coupling force coeff. of roll into sway,} \tag{4.25}$$

ϕ_A=5°, 10°, 15° Rolling amplitude.

4.4 Comparison the experimental results with the calculated results

The calculated results and the experimental results obtained by the above mentioned method are shown in Fig. 4.6~Fig. 4.35.

(i) Added mass coefficient for heave: $\hat{M}_H$

$\hat{M}_H$ increases in the full frequency range as the depth of water becomes shallow. This tendency is agreement with the Tasai and Kim's result [28] which shows that the heaving natural period of ship becomes large as the depths of water become shallow. In the range of low frequency $\hat{M}_H$ of infinite depth increases in a logarithmic way, but $\hat{M}_H$ of finite depths for $KT\to 0$ yield finite values respectively according to our calculations and experiments. Sayer and Ursell have calculated $\hat{M}_H$ of semi-circular at $KT=0$ as for this characteristic [3]. The calculated results are larger than the experimental results at very shallow water, but the tendencies of both are in good agreement. (Fig. 4.6)

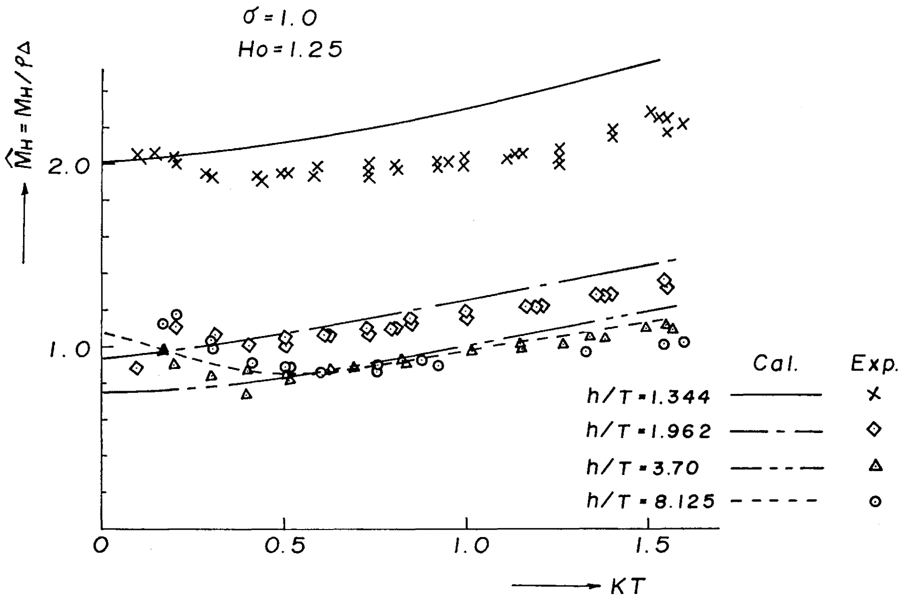

Fig. 4.6 $\hat{M}_H$: Added mass coeff. of heave for rectangular cylinder

(ii) Damping coefficient for heave: $\hat{N}_H$ and wave amplitude ratio: $\hat{A}_H$

$\hat{N}_H$ increases in the full frequency range as the depths of water become shallow. The wave amplitude ratios $\hat{A}_H$ also have similar tendencies. Since the damping coefficient obtained by the potential theory is all compose of the wave damping force, the damping coefficient $\hat{N}_H$ at $KT=0$ has to yield to zero because of $\hat{A}_H=0$. But since the gradient of $\hat{A}_H$ at $KT=0$ becomes large as the depths of water become shallow shown in Fig. 4. 8, $\hat{N}_H$ does not yield the zero value near at $KT=0$ shown in Fig. 4. 7 that is different from one of other oscillating mode. This characteristic is comfirmed by calculating very near at zero frequency $KT=0$. The calculated results of the damping coefficients and the wave amplitude ratios are in good agreement with the experimental results.

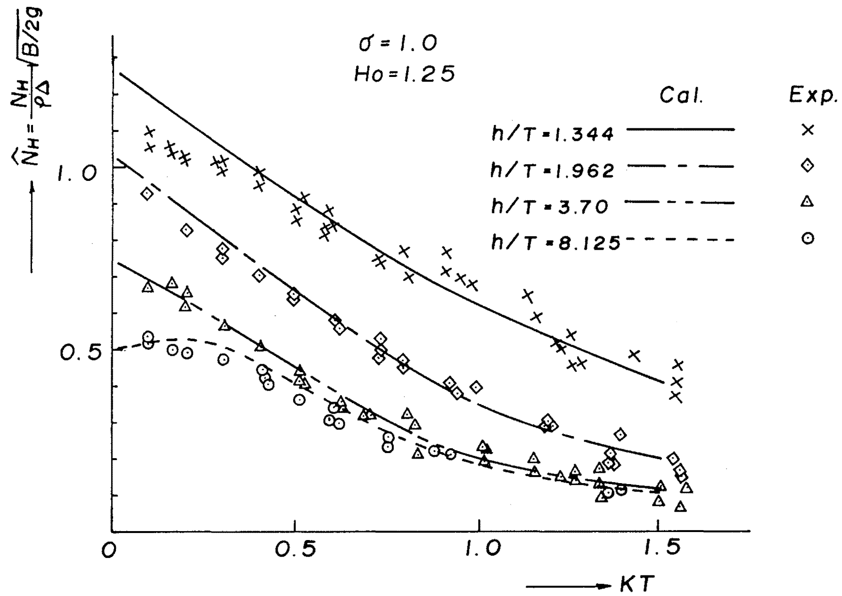

Fig. 4. 7 $\hat{N}_H$: Damping coeff. of heave for rectangular cylinder

(iii) Added mass coefficient for sway: M_S

$\hat{M}_S$ decreases generally as the depths of water become shallow, but increases coversely in the range of low frequency as the depths of water become shallow. The above tendency is independent on the cross sectional form of cylinder and appears uniformly. As shown in Fig. 4. 9, 4. 10 and 4. 11, the numerical results agree well with the experimental results.

(iv) Damping coefficient for sway: $\hat{N}_s$

$\hat{N}_s$ increases in the range of low frequency as the depths of water become shallow but has a tendency decreasing conversely in the range of high frequency as the depths of water become shallow. The rectangular model especially of which beam draft ratio H_0 and the sectional area coefficient σ are larger than those of semicircular model shows intensely the above tendency. Because the wave amplitude ratios become large in the range of high frequency as the depths of water become shallow (Fig. 4. 17), when H_0 and σ of the cross section become large. The theoretical calculations coincide with the

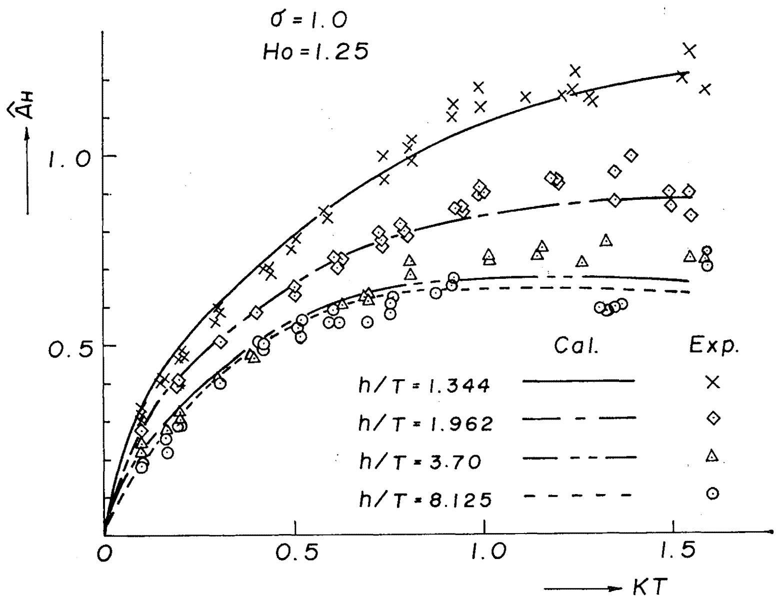

Fig. 4.8 $\hat{A}_H$: Wave amplitude ratio of heave for rectangular cylinder

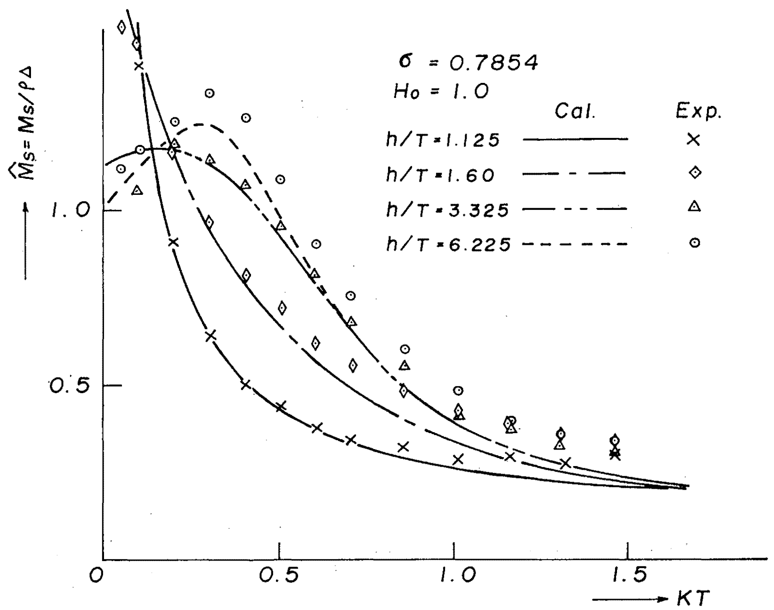

Fig. 4.9 $\hat{M}_s$: Added mass coeff. of sway for semi-circular cylindr

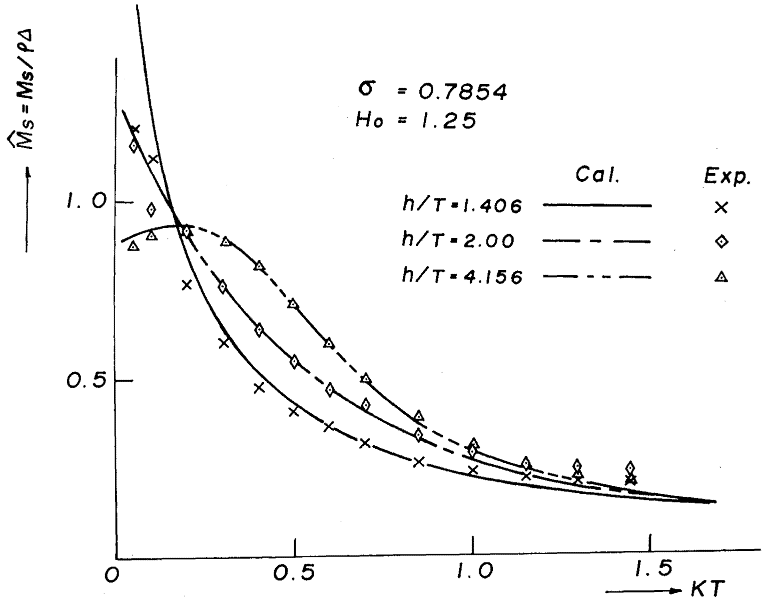

Fig. 4.10 $\hat{M}_s$: Added mass coeff. of sway for elliptical cylinder

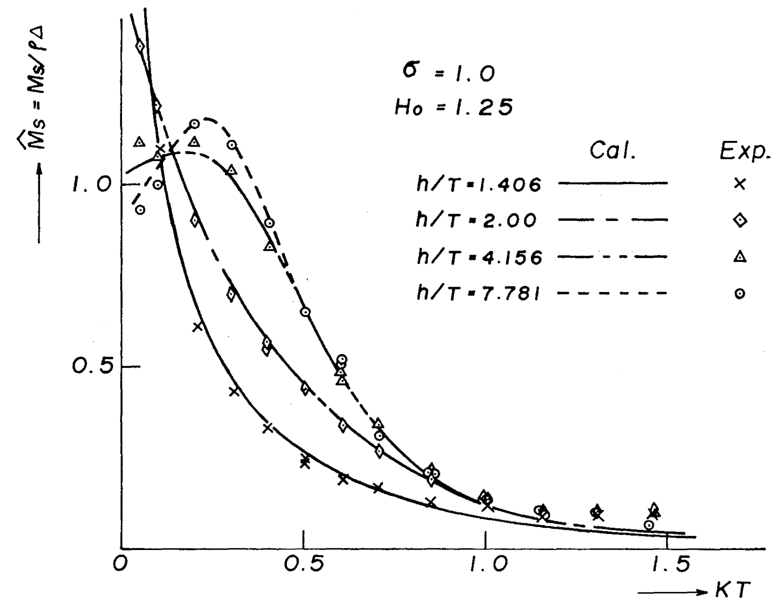

Fig. 4.11 $\hat{M}_s$: Added mass coeff. of sway for rectangular cylinder

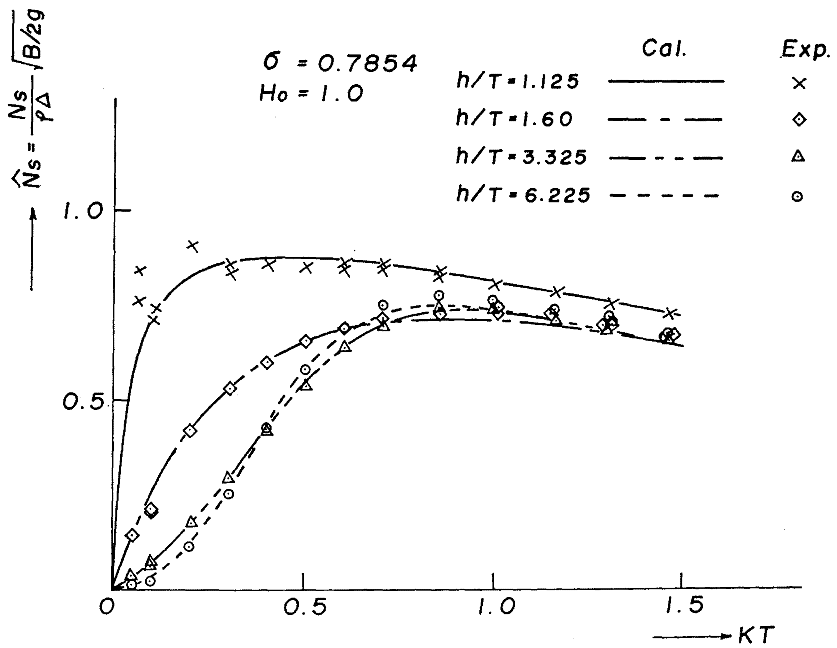

Fig. 4.12 $\hat{N}_s$: Damping coeff. of sway for semi-circular cylinder

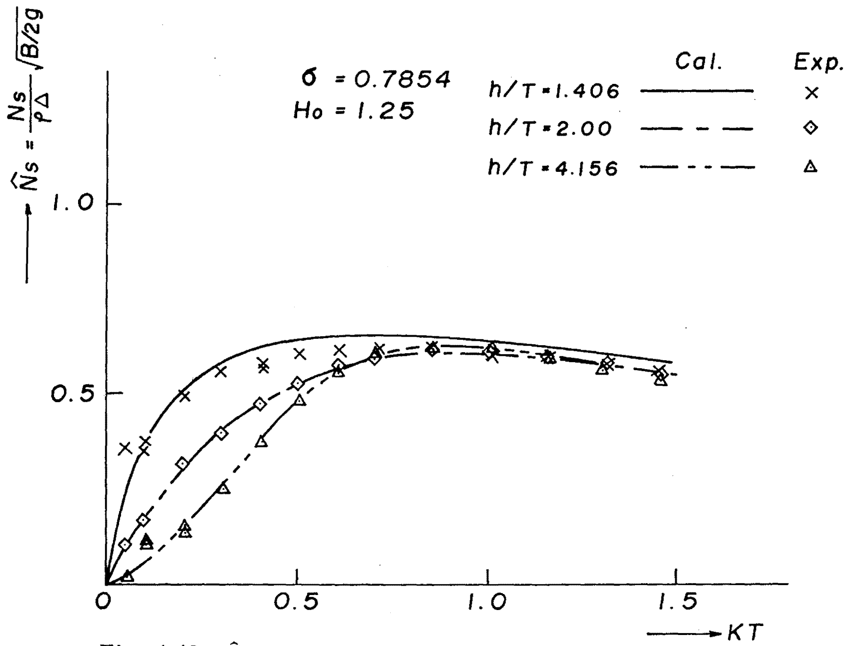

Fig. 4.13 $\hat{N}_s$: Damping coeff. of sway for elliptical cylinder

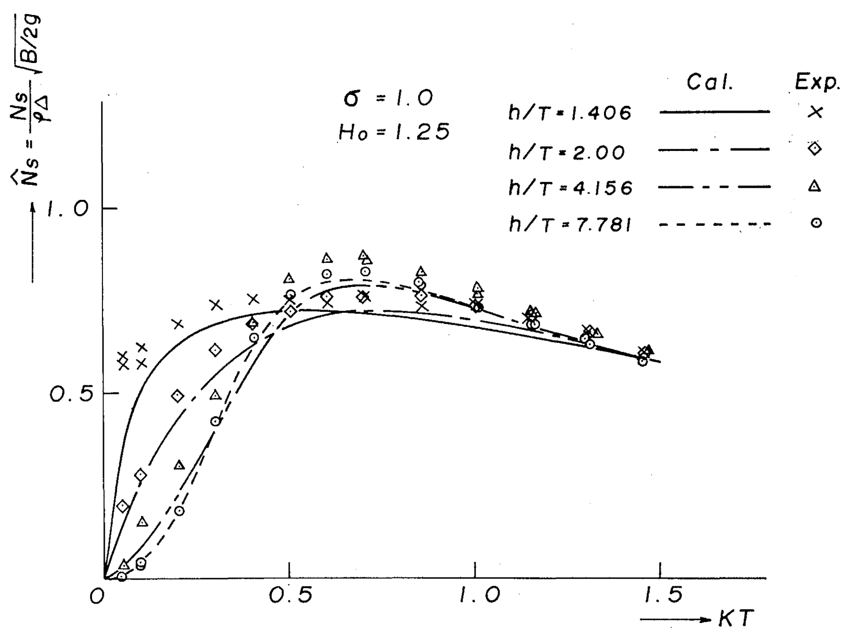

Fig. 4.14 $\hat{N}_S$: Damping coeff. of sway for rectangular cylinder

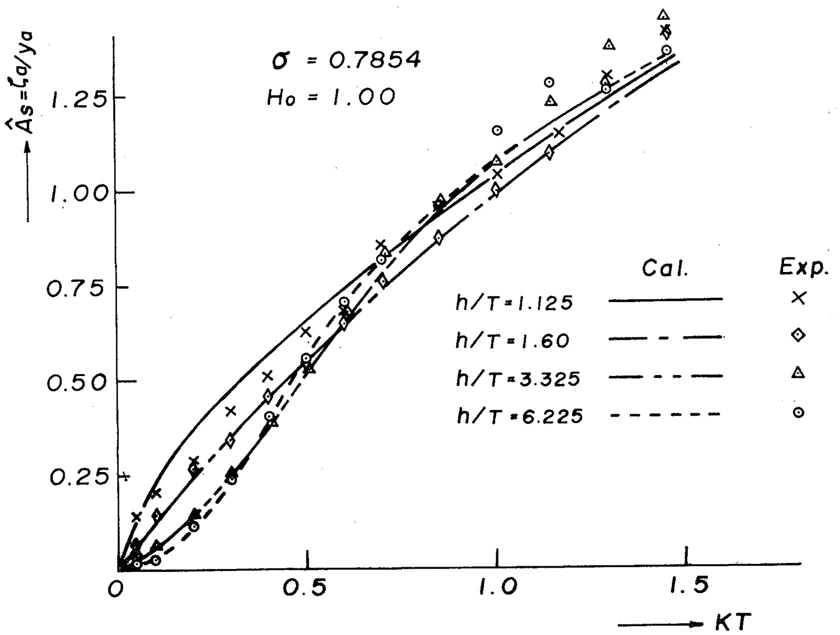

Fig. 4.15 $\hat{A}_S$: Wave amplitude ratio of sway for semi-circular cylinder

experimental results shown in Fig. 4.12, 4.13 and 4.14.

(v) Wave amplitude ratio for sway: $\hat{A}_s$

The tendency of $\hat{A}_s$ with respect to the depths of water is completely similar to that of the damping coefficient composed of the wave damping force which increases in the range of low frequency and decreases conversely in the range of high frequency as the depths of water become shallow. The experimental values show a little scattering, but the calculated results are in fair agreement with the experimental values shown in Fig. 4.15, 4.16 and 4.17.

(vi) Added mass moment of inertia coefficient for roll: $\hat{M}_R$

Since the virtual mass moment of inertia $(J_\phi+M_R)$ composed of the mass moment of inertia J_ϕ and the added mass moment of inertia M_R has been measured by the forced rolling test, it is better to indicate the virtual mass moment of inertia $(J_\phi+M_R)$ than the added mass moment of inertia M_R because of involving the analytical error. So the figures show the virtual mass moment of inertia coefficient $(\hat{J}_\phi+\hat{M}_R)$.

Fig. 4.18 shows the virtual mass momement of inertia coefficients of semi-circular cylinder. In the case of the semi-circular cylinder without a

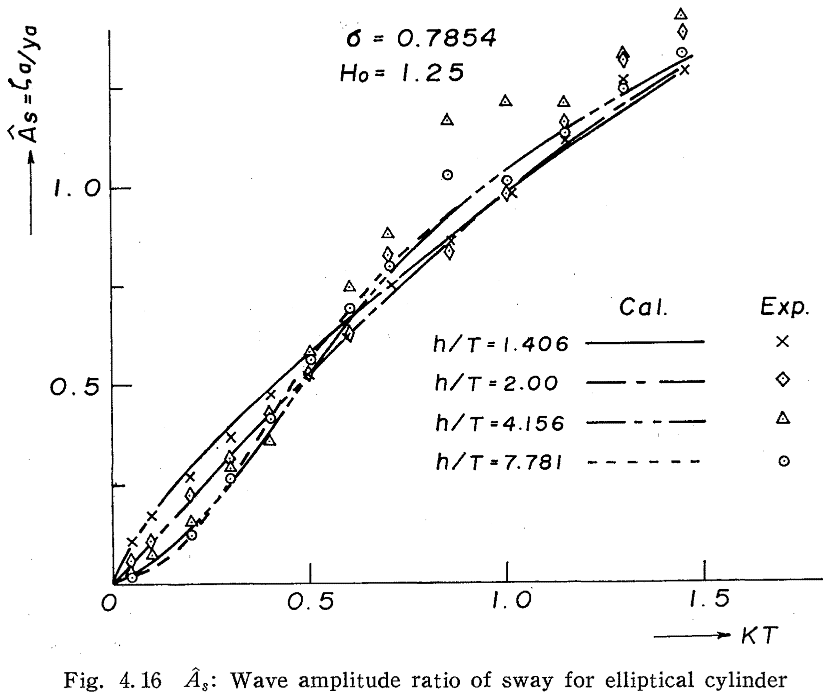

Fig. 4.16 $\hat{A}_s$: Wave amplitude ratio of sway for elliptical cylinder

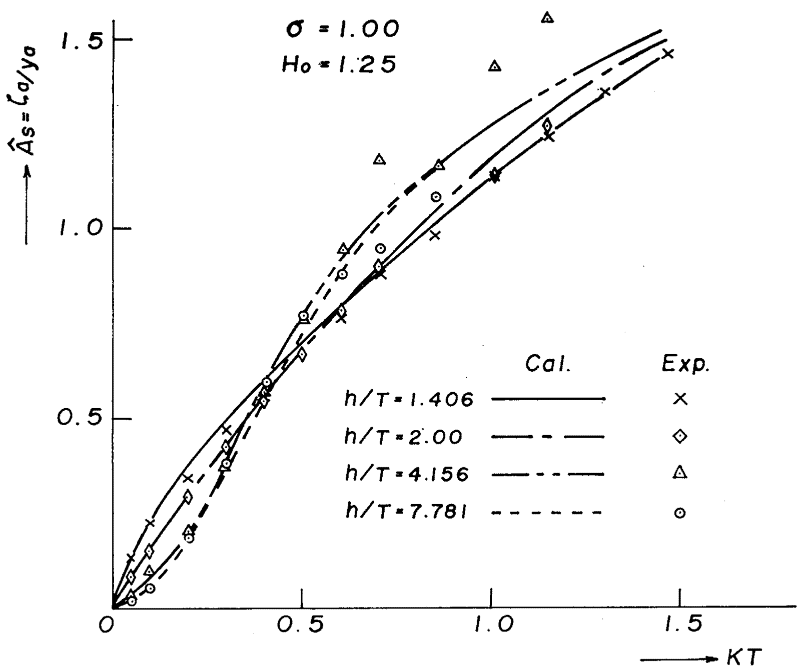

Fig. 4.17 $\hat{A}_s$: Wave amplitude ratio of sway for rectangular cylinder

bilge-keel rolling about the center of the circular O, the added mass moment of inertia obtained by the potential theory is equal to zero and then the virtual mass moment of inertia for roll coincides with the mass moment of inertia of the cylinder. The experiments of the conditions with a bilge-keel ($b_{BK.}=10$ mm) and without a bilge-keel have been carried out. The virtual mass moment of inertia of the semi-circular cylinder without a bilgekeel obtained by the experiments agrees almost with that obtained by the potential theory in the water of deep depth ($h/T=6.225$). The virtual mass moment of inertia of the semi-circular cylinder with a bilge-keel, however, increases rapidly in the range of low frequency as the depths of water become shallow. In the forced rolling tests by Vugts [29], it has been seen that when the rolling amplitude ϕ_A is changed, the added mass moment of inertia M_R decreases in the case of the small rolling amplitude, on the other hand, in the case of the large rolling amplitude M_R increases in the range of low frequency. He has explained these phenomena to be caused by his experimental error. But it seems that these phenomena caused by the viscous effect of the fluid, because the radius of transverse gyration and the center of gravity of this cylinder are constant at the variable depths of water in our experiment and the above tendency appears more strongly in the case that the bilge-keel is set and the depths of water become sha-

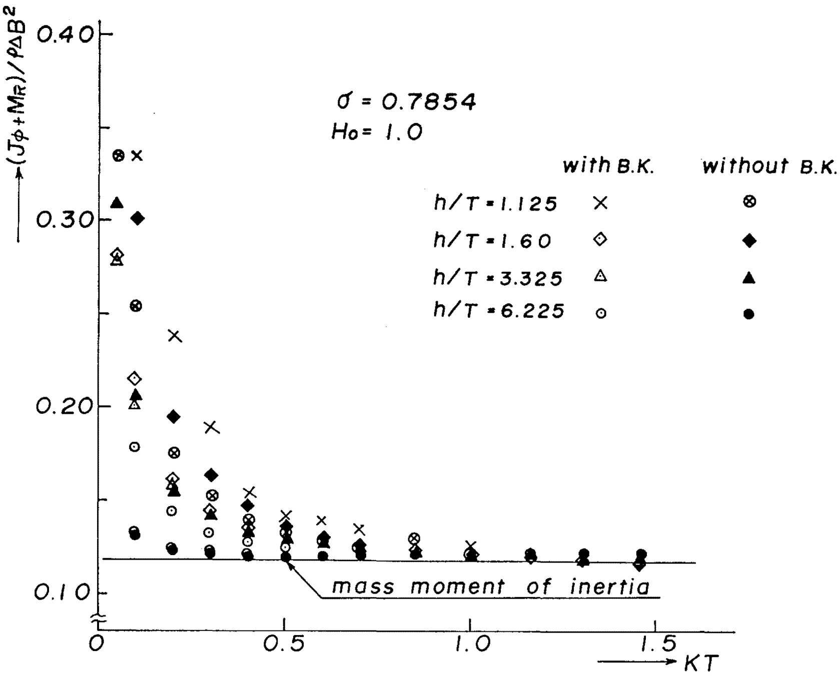

Fig. 4.18 $\hat{J}_\phi+\hat{M}_R$: Virtual mass moment of inertia coeff. for semi-circular cylinder with and without bilge-keel

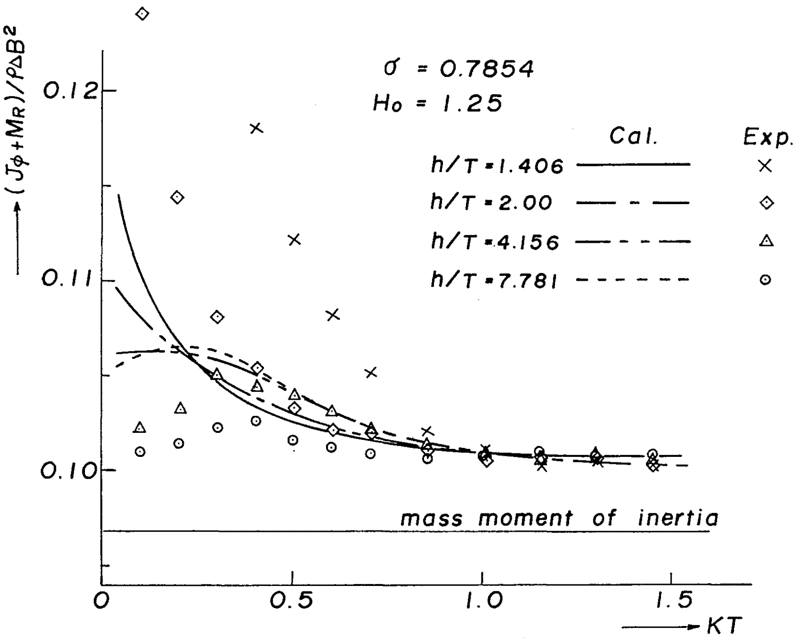

Fig. 4.19 $\hat{J}_\phi+\hat{M}_R$: Virtual mass moment of inertia coeff. for elliptical cylinder without bilge-keel

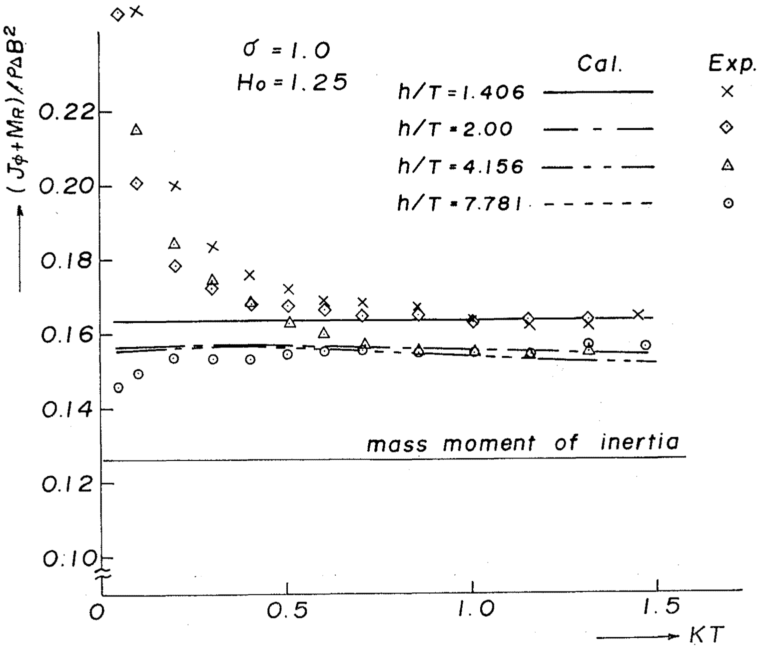

Fig. 4.20 $\hat{J}_\phi+\hat{M}_R$: Virtual mass moment of inertia coeff. for rectangular cylinder with bilge-keel

llow much more. it however seems to be problem which we ought to study hereafter.

The tendency that the added mass moment of inertia M_R increases in the range of low frequency as the depths of water become shallow appears in the experiment of the elliptical cylinder and the rectangular cylinder in shown Fig. 4.19 and 4.20. But the theoretical calculations are in agreement with the experimental results in the range of high frequency. It is seen that M_R increases as the depths of water become shallow and the cross sectional form becomes full according to these figures. The added mass moment of inertia of the rectangular cylinder especially increases in overall range of oscillating frequency as the depths of water become shallow. The above phenomena coincide with those of Iwai's experiments [30] in which the natural period of rolling becomes large as the depths of water become shallow and the block coefficient of ship body becomes large.

(vii) Damping coefficient for roll: $\hat{N}_R$

As the example of the condition without a bilge-keel the wave amplitude ratios of the rolling elliptical cylinder are shown in Fig. 4.21. The tendency as for the effect of depths of water is the same as that of the swaying: the

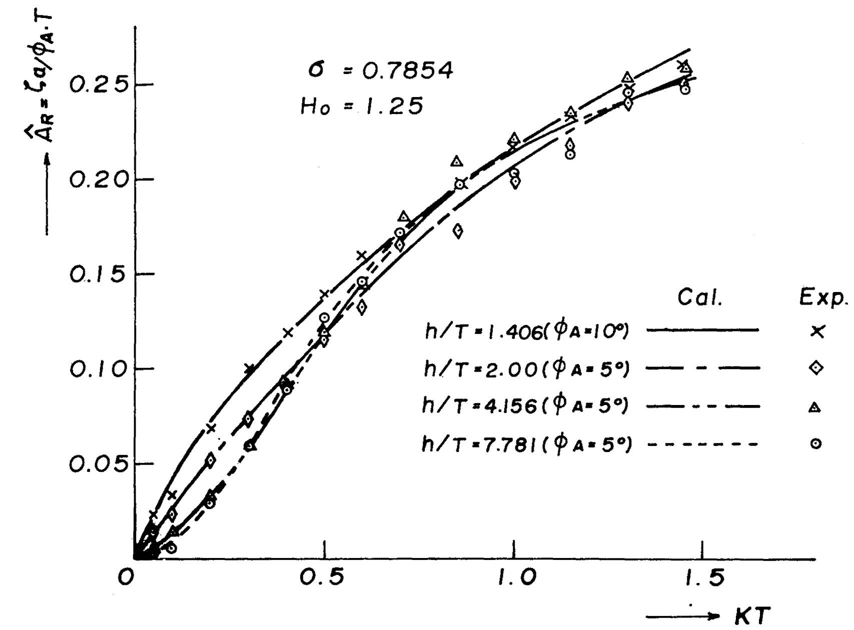

Fig. 4.21 $\hat{A}_R$: Wave amplitude ratio of roll for elliptical cylinder without bilge-keel

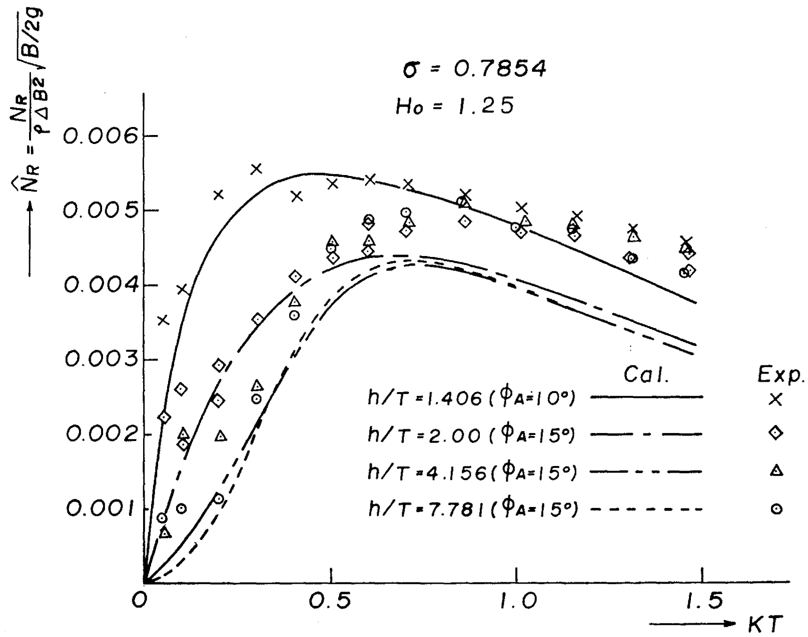

Fig. 4.22 $\hat{N}_R$: Damping coeff. of roll for elliptical cylinder without bilge-keel

wave amplitude ratio $\hat{A}_R$ becomes large in the range of low frequency and becomes small conversely in the range of high frequency as the depths of water become shallow. The theoretically calculated values are in good agreement with the experimental values as shown in Fig. 4. 22. Since the damping coefficient of the rolling elliptical cylinder without bilge-keel $\hat{N}_R$ is almost composed of the component of wave damping force and does not involve almost the component of viscous effect of fluid in the range of low frequency, it can be estimated by the potential theory. The viscous damping component, however, becomes much as the oscillating frequency becomes to the range of high frequency, and the rolling damping components become to be composed of the components of the wave damping force and the viscous damping force in the range of high frequency. And the rolling damping values obtained by the experiments are much more than the theoretically calculated values obtained by the potential theory and the effect of water depth does not appear clearly in the experimental values at the same time.

In the next place, in order to study the effect of the bilgekeel the forced rolling tests have been carried out by using the semi-circular cylinder with the bilge-keel ($b_{B.K.}=10$ mm). At the first time the wave amplitude ratios of the rolling semi-circular cylinder without a bilge-keel are shown in Fig. 4. 23. According to the potential theory, the wave amplitude ratio of the rolling semi-circular cylinder is equal to zero, but there are outgoing waves actually with aid of the viscous fluid. Krap and Kotick [31] have obtained the following experimental formula which expresses the amplitude of the outgoing wave, when the semi-circular cylinder is rolling about the center of the cylinder O in the water of infinite depth written by

$$\zeta_a=4(Kr)^2\sqrt{\nu/\omega}\cdot\phi_A \tag{4.26}$$

where r: radius of semi-circular cylinder,
ν: fluid kinematic viscosity.

The values of the above formula (4. 26) are represented in Fig. 4. 23. According to this figure it is seen that the wave amplitude ratios $\hat{A}_R$ become larger in the range of low frequency and conversely smaller in the range of high frequency than that of the above formula as the depths of water become shallow in water of finite depth.

As shown in Fig. 4. 24, the wave amplitude ratios of the rolling semi-circular cylinder with the bilge-keel become larger than that without a bilge-keel and the order of the wave amplitude ratios take a figure up one place. And so it is seen that we can't neglect the outgoing wave amplitude by the effect of the bilge-keel and the effects of water depths as for $\hat{A}_R$ become generally large as the depths of water become deep.

The roling damping coefficients $\hat{N}_R$ of these two conditions with and without the bilge-keel are shown in Fig. 4. 25. It is seen from this figure

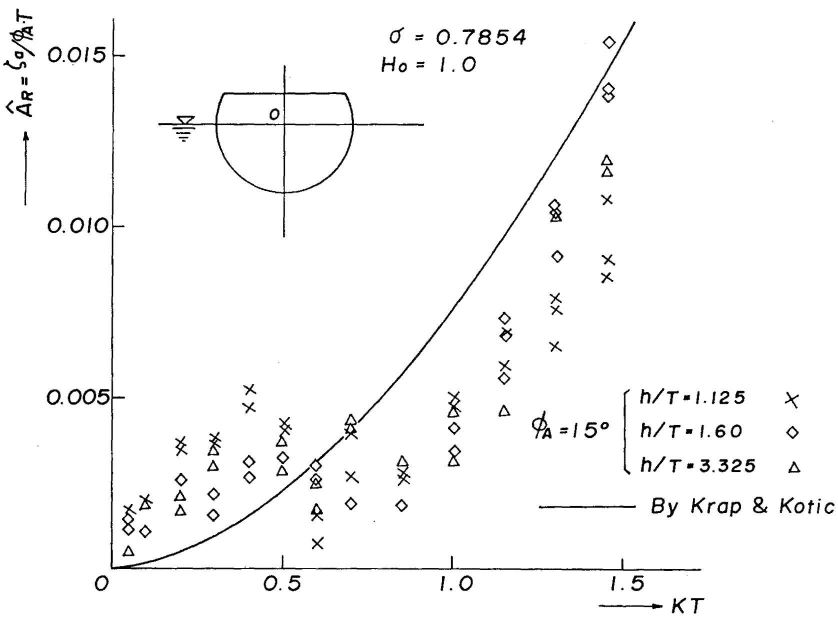

Fig. 4.23 $\hat{A}_R$: Wave amplitude ratio of roll for semi-circular cylinder without bilge-keel

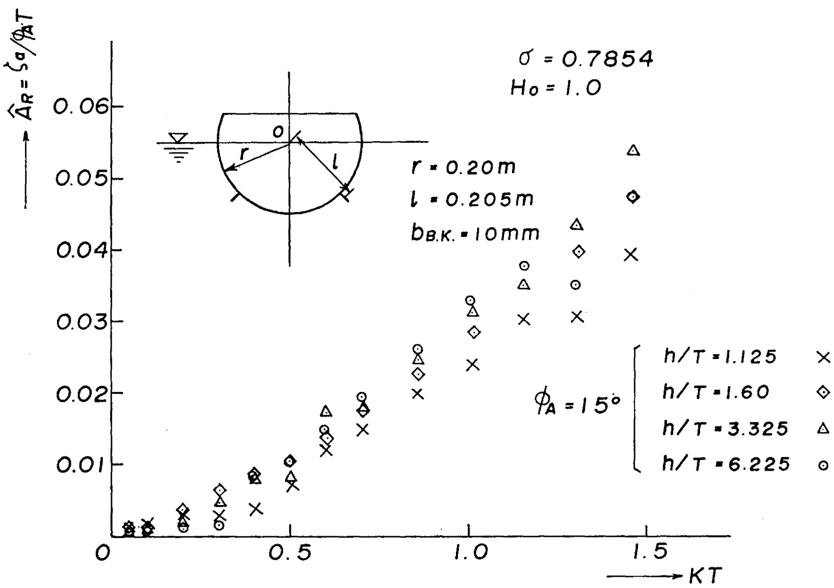

Fig. 4.24 $\hat{A}_R$: Wave amplitude ratio of roll for semi-circular cylinder with bilge-keel

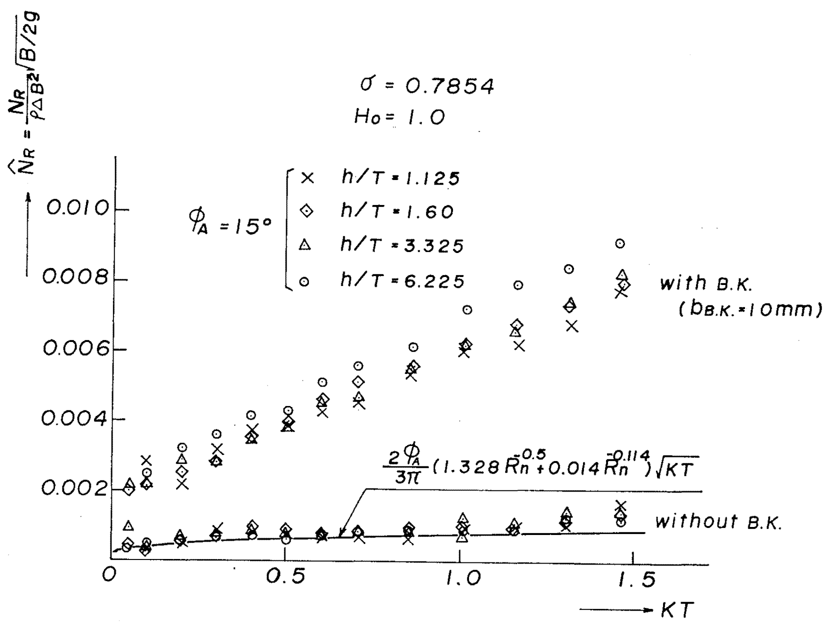

Fig. 4.25 $\hat{N}_R$: Damping coeff. of roll for semi-circular cylinder with and without bilge-keel

that the $\hat{N}_R$ without the bilge-keel are not affected very much the effect of water bottom. We suppose that we neglect the wave damping force without the bilge-keel above mentioned as the small component and the rolling damping forces are completely composed of the frictional damping component. Namely we consider the oscillation of the semi-circular cylinder about the center of the cylinder O and the flat plate in the uniform flow as the same condition and obtain the frictional resistance acting on the flat plate using Hugh's frictional resistance coefficient [32] given as

$$C_f = 1.328 R_n^{-0.5} + 0.014 R_n^{-0.114}. \tag{4.27}$$

where $R_n = \frac{LV}{\nu}$: Reynolds number, L: Length of plate,

$\nu = 1.01 \quad 10^{-6}\text{m}^2/\text{sec}$ (20°C), V: Speed of fluid.

We transform the term of the square of the velocity to the equivalent linear equation as follows:

$$R_f = \frac{1}{2}\rho \cdot C_f \cdot S \cdot V^2 = \frac{1}{2}\rho \cdot C_f \cdot S \cdot |r\dot{\phi}| \cdot r\dot{\phi}$$

$$\doteqdot \frac{1}{2}\rho \cdot C_f \cdot S \cdot \frac{8}{3\pi}\omega^2 r^2 \phi_A{}^2 \cos \omega t. \tag{4.28}$$

where $S=\pi rL$: Surface area of cylinder.

The frictional resistance moment $N_R\cdot\dot{\phi}$ obtained by the above equation are expressed as

$$N_R\cdot\dot{\phi}=L\int_c r\cdot dR_f=\frac{4}{3}\rho C_f\ \omega^2\phi_A{}^2r^4\ L\cos\omega t,$$

$$\therefore N_R=\frac{4}{3}\rho C_f\omega\phi_A r^4 L, \tag{4.29}$$

$$\therefore \hat{N}_R=\frac{N_R}{\rho\Delta B^2}\sqrt{B/2g}=\frac{2\phi_A}{3\pi}(1.328\,R_n{}^{-0.5}+0.014\,R_n{}^{-0.114})\sqrt{KT}, \tag{4.30}$$

where $T=r$: Radius of semi-circular,
$V=\omega\phi_A r$, $\phi_A=15°$: Roll amplitude.

It has become obvious that the values obtained by the formula (4.30) are in good agreement with the experimental values. The rolling damping moments of the semi-circular cylinder with the bilge-keel are not significantly affected the effect of water depth shown in Fig. 4.25. It is necessary to take into account the direct pressures acting on the bilge-keel because the $\hat{N}_R$ with the bilge-keel are larger by taking a figure up one place than that without the bilge-keel.

Fig. 4.26 shows the wave amplitude ratios $\hat{A}_R$ of the rectangular cylinder with the bilge-keel ($b_{B.K.}=10$ mm). The wave amplitude ratios $\hat{A}_R$ of the rectangular cylinder without the bilge-keel, which are shown with a mark (●) in Fig. 4.26, are sufficiently estimated by the potential theory, but the wave amplitude ratios with the bilge-keel become larger than the theoretically calculated values because of the outgoing wave occured by the bilge-keel. The tendencies of $\hat{A}_R$ as for the various depths of water become small constantly as the depths of water become shallow. The rolling damping moment coefficients $\hat{N}_R$ of the rectangular cylinder are shown in Fig. 4.27. The order of the rolling damping moment without bilge-keel obtained by the experiment is almost equal to that obtained by the potential theory. On the other hand the order of the rolling damping moment with the bilge-keel takes a figure up one place. Furthermore it is an interesting problem that the rolling damping moments are not affected very much the effect of water bottom until the ratio of water depth and draft h/T becomes to be equal to about twice, but the $\hat{N}_R$ increase rapidly and the values with the rolling amplitude $\phi_A=10°$ are equal to those with the rolling amplitude $\phi_A=15°$ as the depth of water becomes very shallow $h/T=1.406$.

The effects of water depth as to the rolling damping coefficients obtained from these experimental results may be summarized as follows.

(a) The component of the wave damping force is affected significantly the effects of water depths, and it is not able to neglect the wave damping

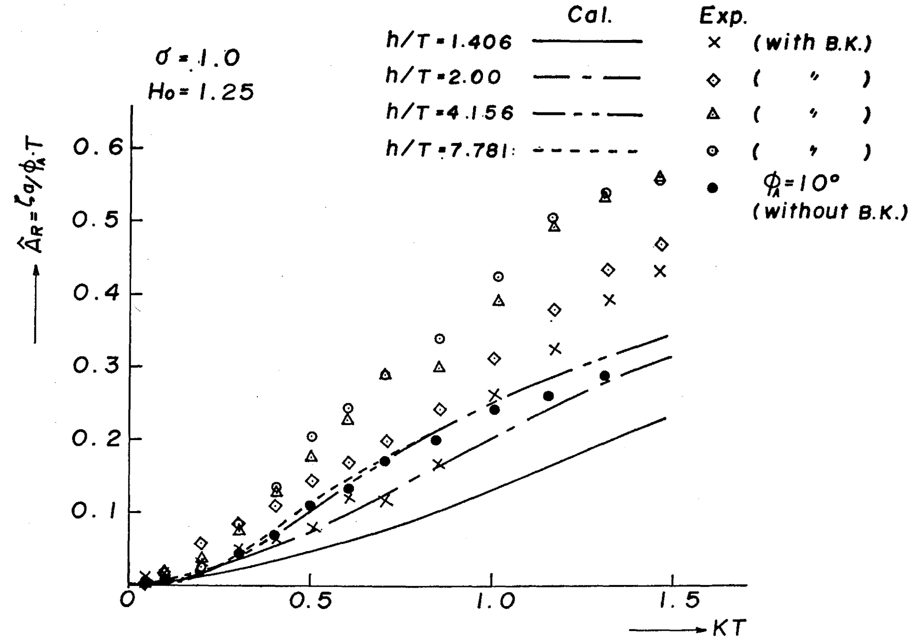

Fig. 4.26 $\hat{A}_R$: Wave amplitude ratio of roll for rectangular cylinder with bilge-keel

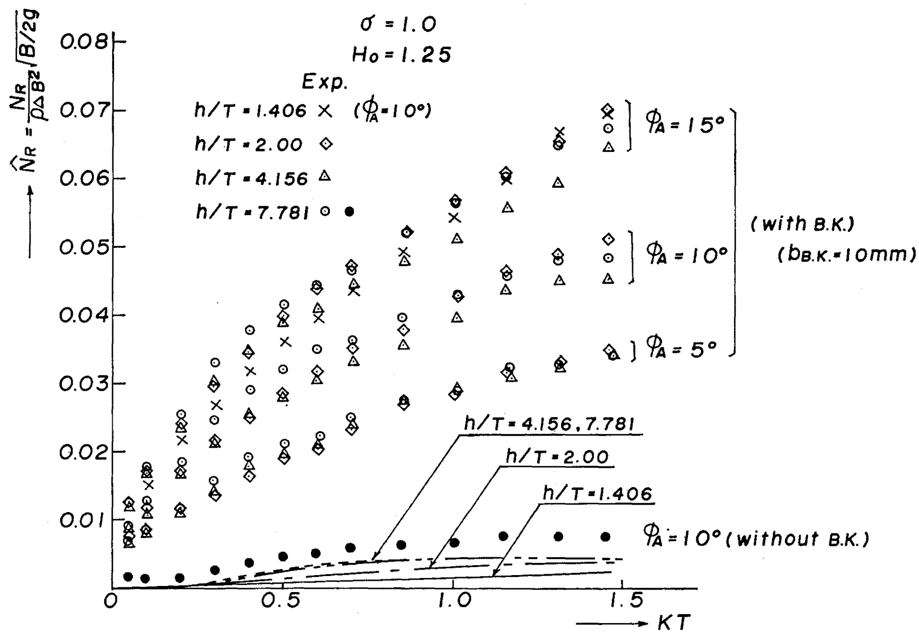

Fig. 4.27 $\hat{N}_R$: Damping coeff. of roll for rectangular cylinder with bilge-keel

force occured by the bilge-keel.

(b) The firictional damping component and the direct pressures acting on the bilge-keel within the viscous components are not affect the effect of water depth at all.

(c) The pressure distributions on the surface of the cylinder occured by the bilge-keel do not change until the ratio of the water depth and the draft is equal to twice ($h/T=2.0$) and then change very much and produce a large pressure damping force as the depth of water becomes very shallow ($h/T=1.4$).

(viii) Cross coupling terms: $\hat{M}_{\eta\phi}=\hat{M}_{\phi\eta}$, $\hat{N}_{\eta\phi}=\hat{N}_{\phi\eta}$

Firstly the symmetric relations of cross coupling term $\hat{M}_{\eta\phi}=\hat{M}_{\phi\eta}$ and $\hat{N}_{\eta\phi}=\hat{N}_{\phi\eta}$ of the elliptical cylinder without a bilgekeel are satisfied and the numerically calculated results almost agree with the experimental results shown in Fig. 4.28, 4.29, 4.30 and 4.31. The tendencies of cross coupling terms as to the various depths of water are similar very much to those of the added mass and the damping coefficients for the swaying elliptical cylinder respectively.

In the next place, the symmetric relation of cross coupling term $\hat{M}_{\eta\phi}=\hat{M}_{\phi\eta}$

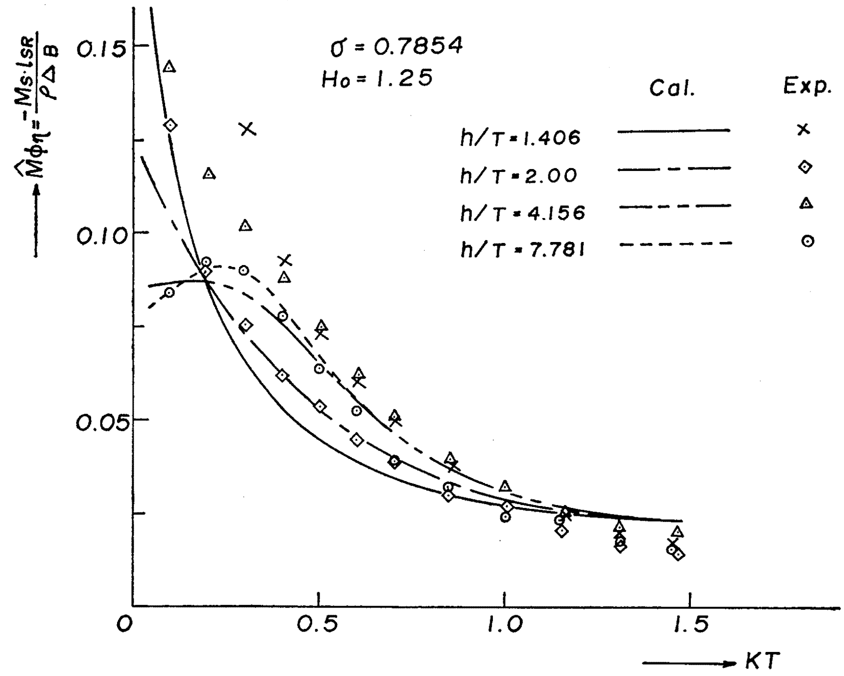

Fig. 4.28 $\hat{M}_{\phi\eta}$: Coupling force coeff. of roll into sway for elliptical cylinder without bilge-keel

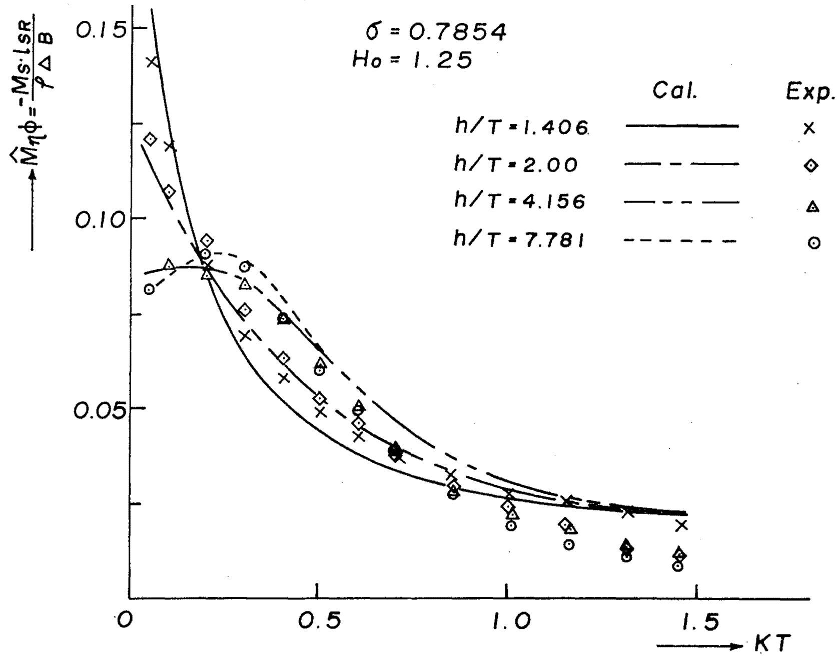

Fig. 4.29 $\hat{M}_{\eta\phi}$: Coupling moment coeff. of sway into roll for elliptical cylinder without bilge-keel

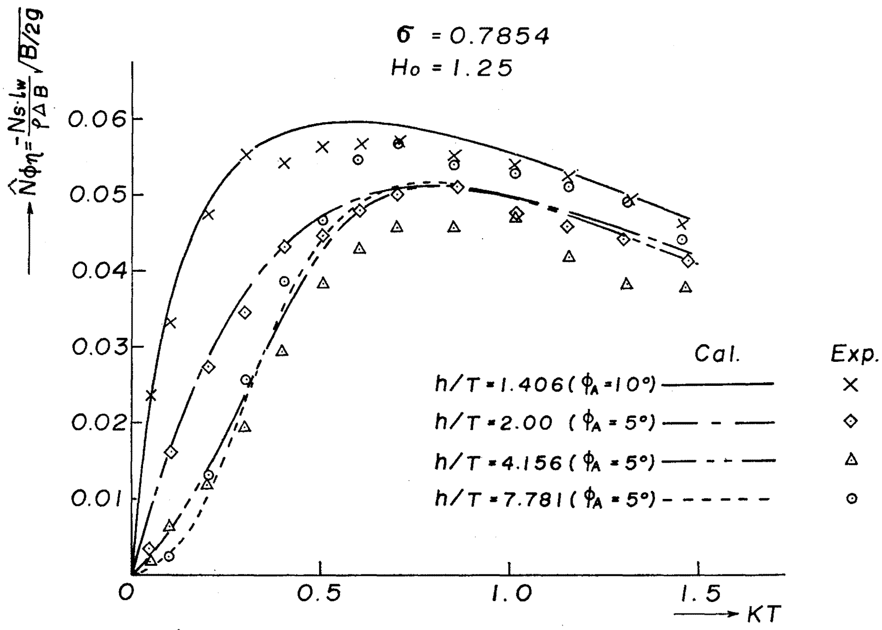

Fig. 4.30 $\hat{N}_{\phi\eta}$: Coupling force coeff. of roll into sway for elliptical cylinder without bilge-keel

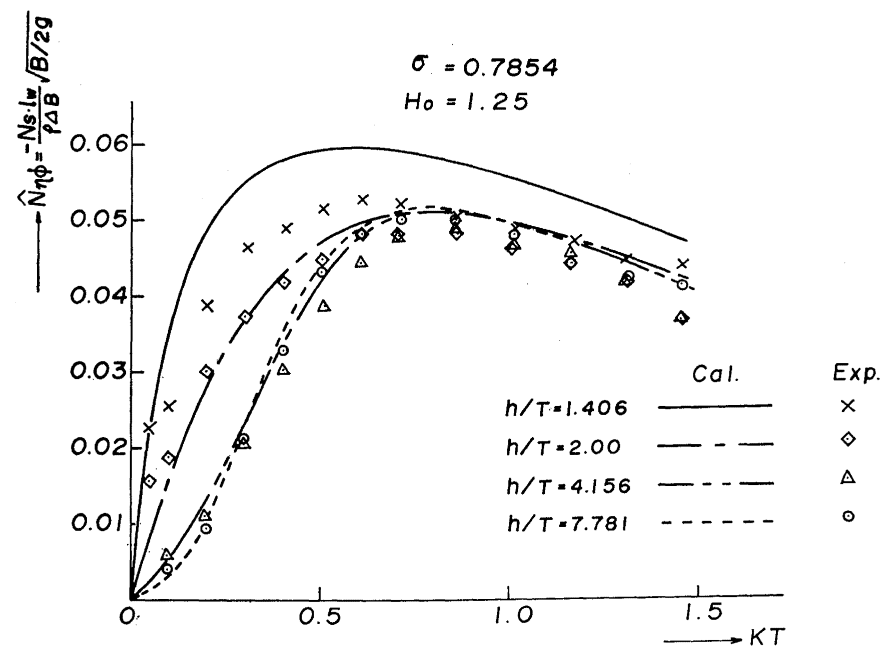

Fig. 4.31 $\hat{N}_{\eta\phi}$: Coupling moment coeff. of sway into roll for elliptical cylinder without bilge-keel

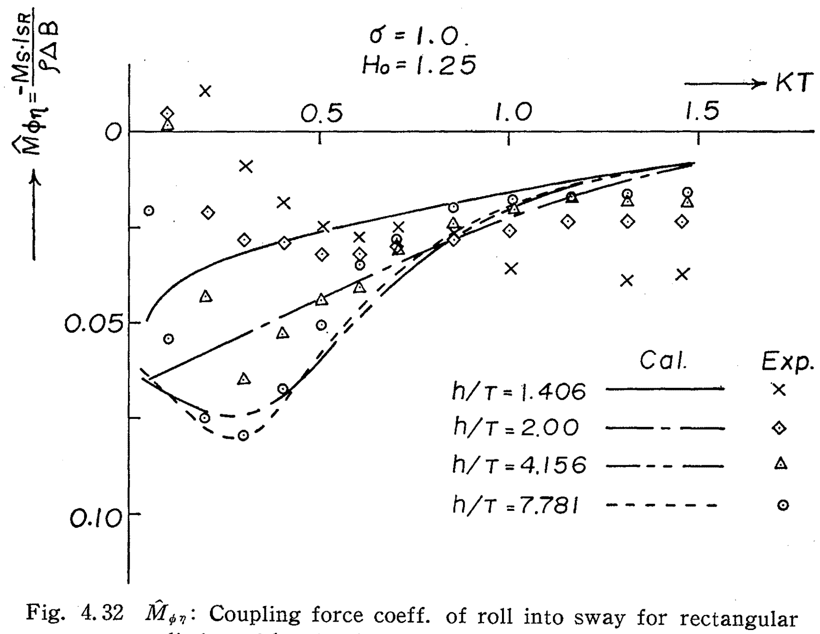

Fig. 4.32 $\hat{M}_{\phi\eta}$: Coupling force coeff. of roll into sway for rectangular cylinder with bilge-keel

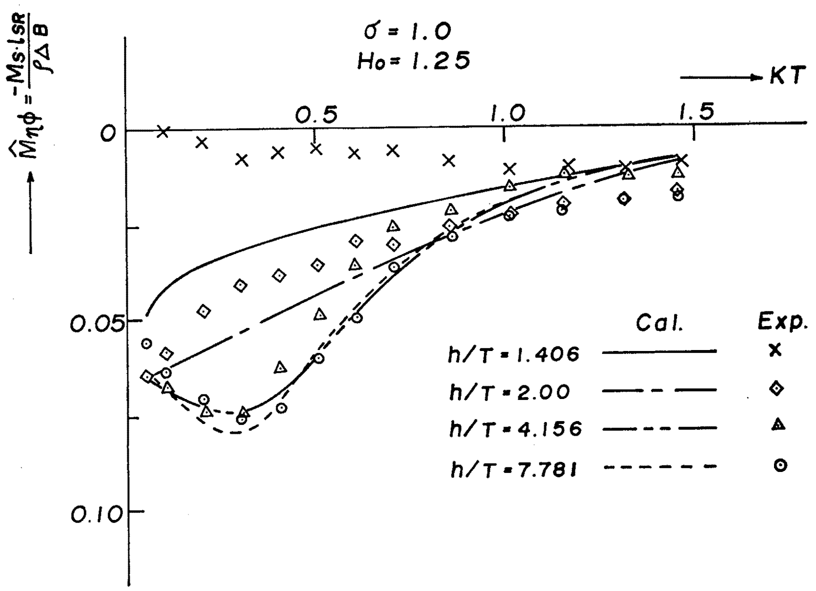

Fig. 4.33 $\hat{M}_{\eta\phi}$: Coupling moment coeff. of sway into roll for rectangular cylinder with bilge-keel

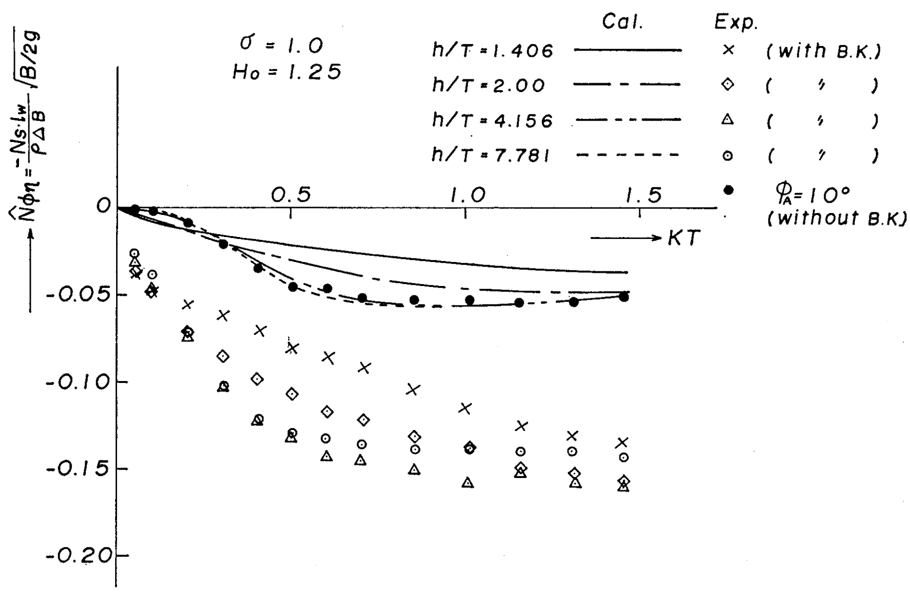

Fig. 4.34 $\hat{N}_{\phi\eta}$: Coupling force coeff. of roll into sway for rectangular cylinder with bilge-keel

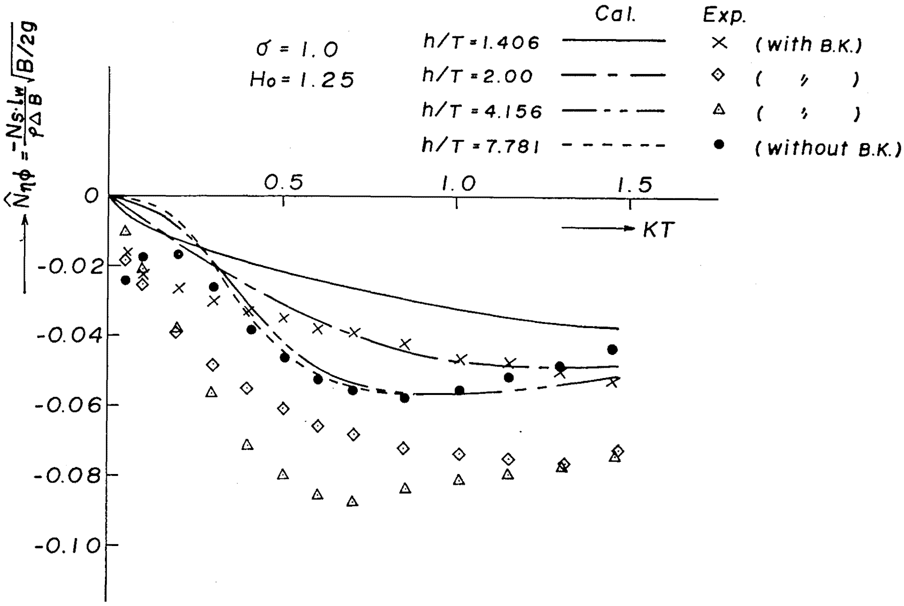

Fig. 4.35 $\hat{N}_{\eta\phi}$: Coupling moment coeff. of sway into roll for rectangular cylinder with bilge-keel

of the rectangular cylinder with the bilge-keel ($b_{B.K.}=10$ mm) is satisfied in comparatively shallow water. But the theoretically calculated values do not coincide with the experimental values as the depths of water become very shallow shown in Fig. 4.32 and 4.33.

The experimental results without the bilge-keel satisfy the symmetric relation $\hat{N}_{\eta\phi}=\hat{N}_{\phi\eta}$ and are in good agreement with the theoretically calculated results. But the absolute values of the experimental results with the bilge-keel are larger than the numerically calculated absolute values. Especially the coupling terms $\hat{N}_{\eta\phi}$ of the rolling into the swaying become large. The bilge-keel affects very much not only the rolling damping moment but also the coupling terms which are proportional to the velocity shown in Fig. 4.34 and 4.35.

4.5 Examples of numerical calculations

(i) Comparison with Kim's results

C. H. Kim has calculated the hydrodynamic forces and moments acting on the rectangular cylinder[4], which has a Lewis form cross section with the sectional area coefficient $\sigma=1.0$ and the beamdraft ratio $H_0=1.0$, by using the method of multipole expansions. The results comparing our values with

Kim s values are shown in Fig. 4. 36~Fig. 4. 43.

As for the heaving added mass coefficients $\hat{M}_H$ shown in Fig. 4. 36 Kim's results are very different from ours in the range of low frequency, because Kim has mistaken the mesh size to calculate the infinite integral equations (4. 13) and (4. 16) in the previous section. There is no great difference between our results and Kim's results, which are the wave amplitude ratios $\hat{A}_H$ except for the case of $h/T=2.0$ as shown in Fig. 4. 37.

As for the hydrodynamic force and moment of the swaying, the rolling and the cross coupling, there are little difference except for the coupling moment lever l_{SR} which is proportional to acceleration as shown in Fig. 4. 42.

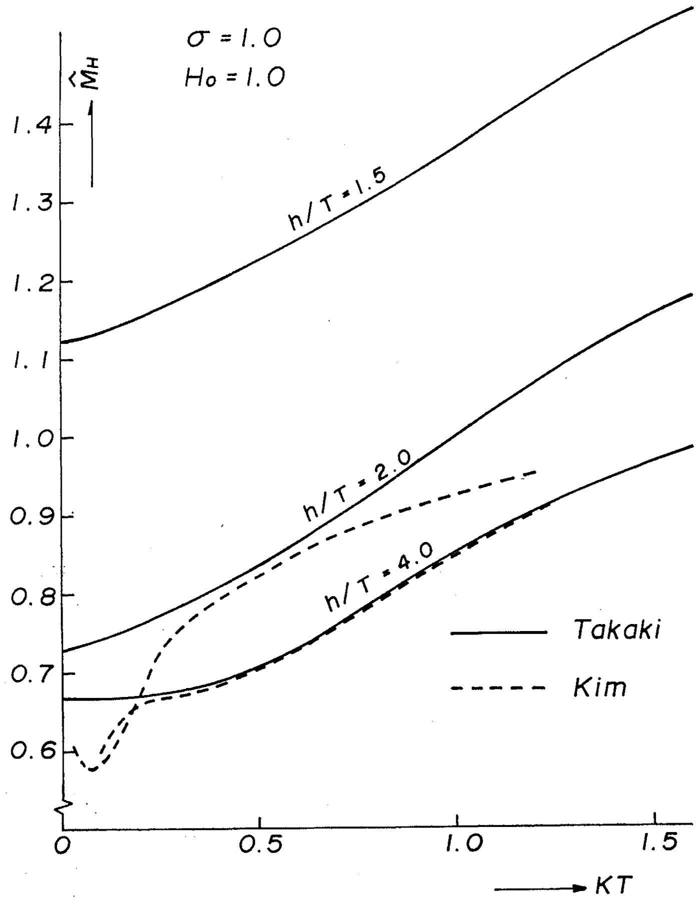

Fig. 4. 36 $\hat{M}_H$: Added mass coeff. of heave for rectangular cylinder

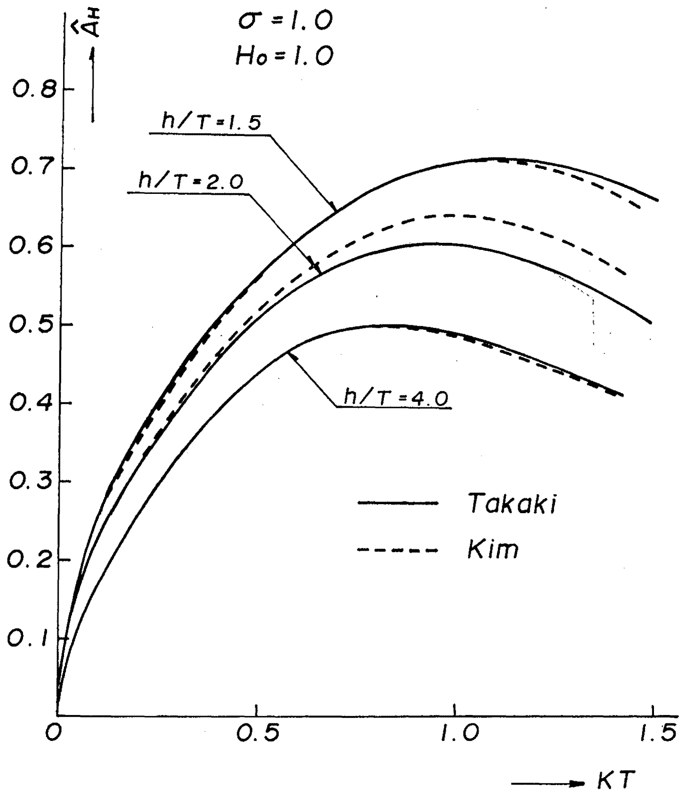

Fig. 4.37 $\hat{A}_H$: Wave amplitude ratio of heave for rectangular cylinder

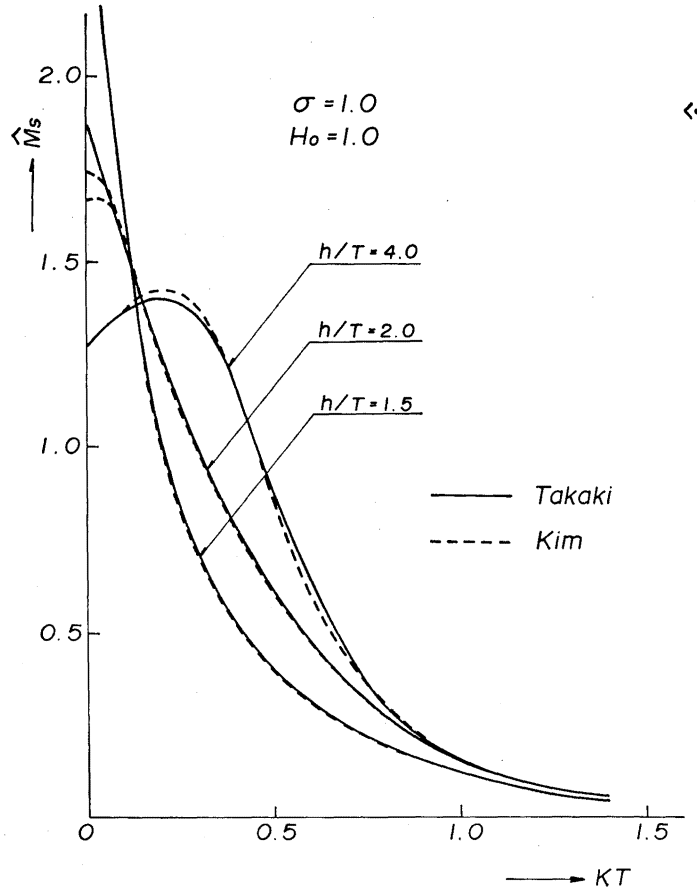

Fig. 4.38 $\hat{M}_s$: Added mass coeff. of sway for rectangular cylinder

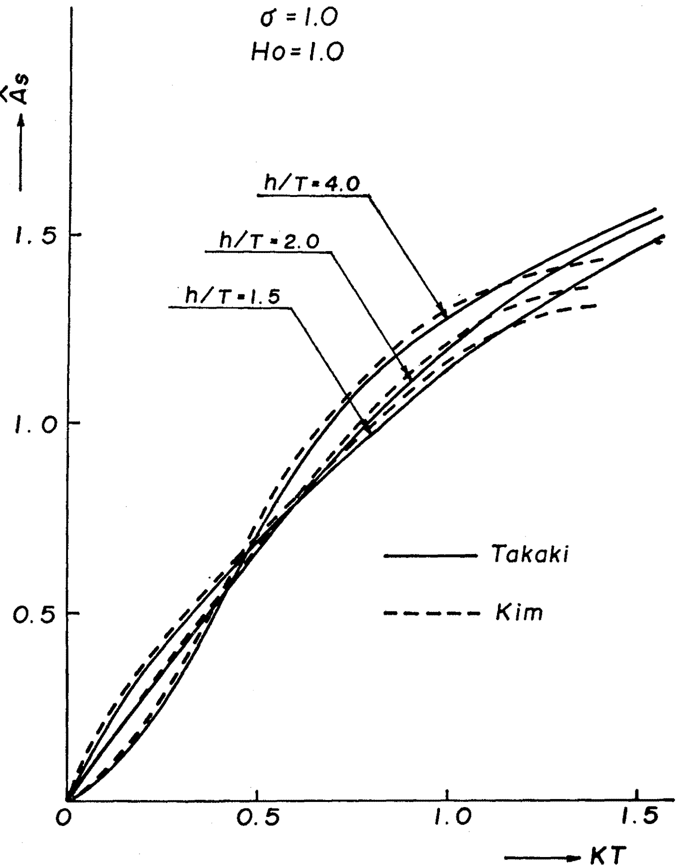

Fig. 4.39 $\hat{A}_s$: Wave amplitude ratio of sway for rectangular cylinder

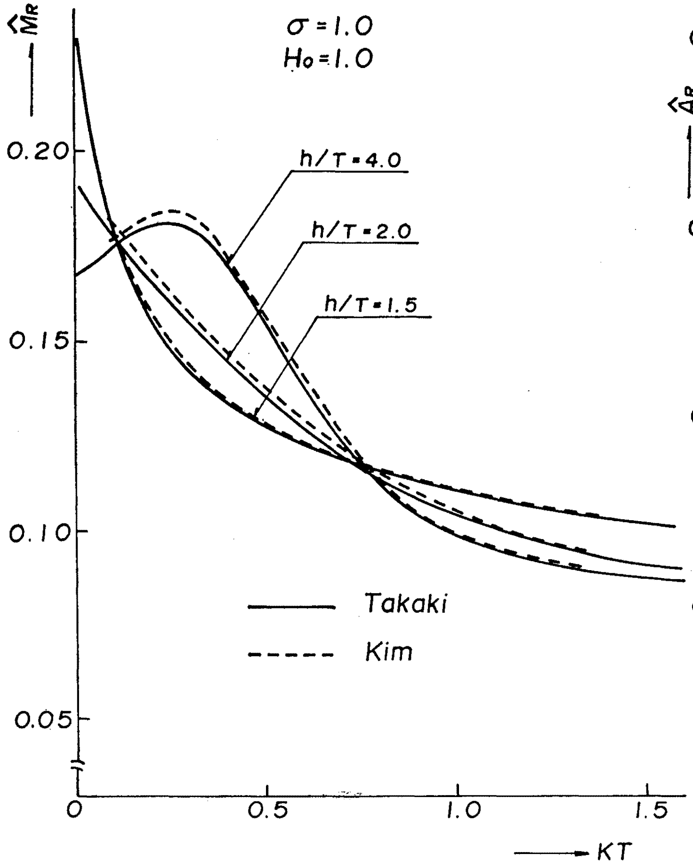

Fig. 4.40 $\hat{M}_R$: Added mass moment of inertia coeff. of roll for rectangular cylinder

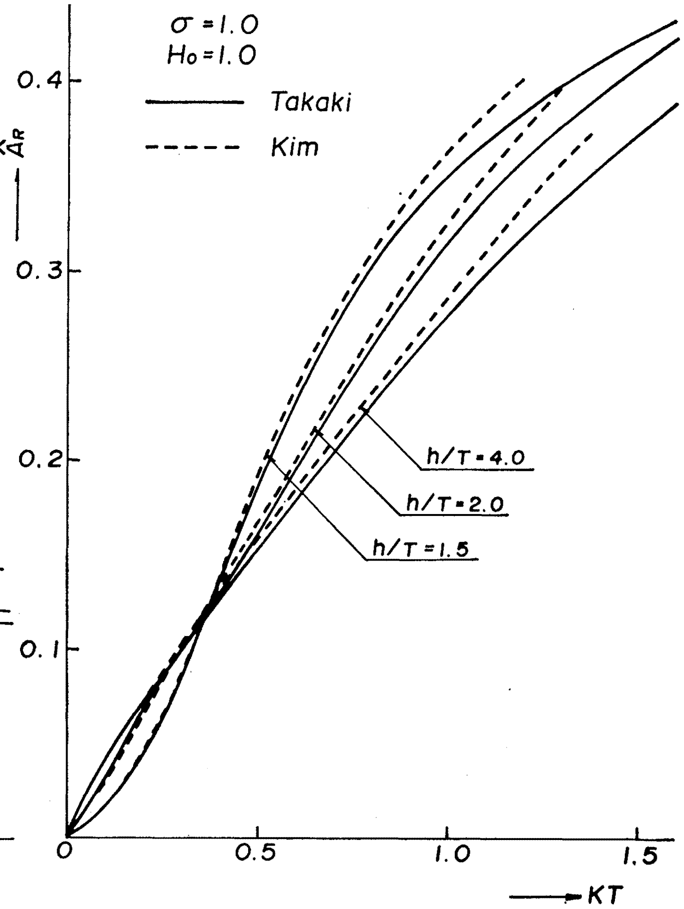

Fig. 4.41 $\hat{A}_R$: Wave amplitude ratio of roll for rectangular cylinder

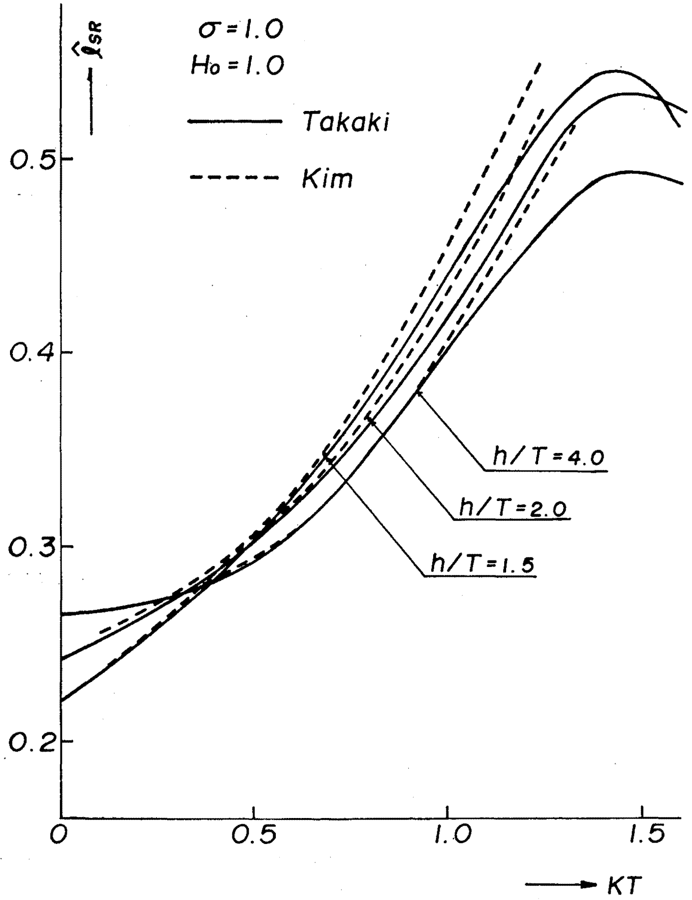

Fig. 4.42 $\hat{l}_{sR}$: Added moment arm for rectangular cylinder

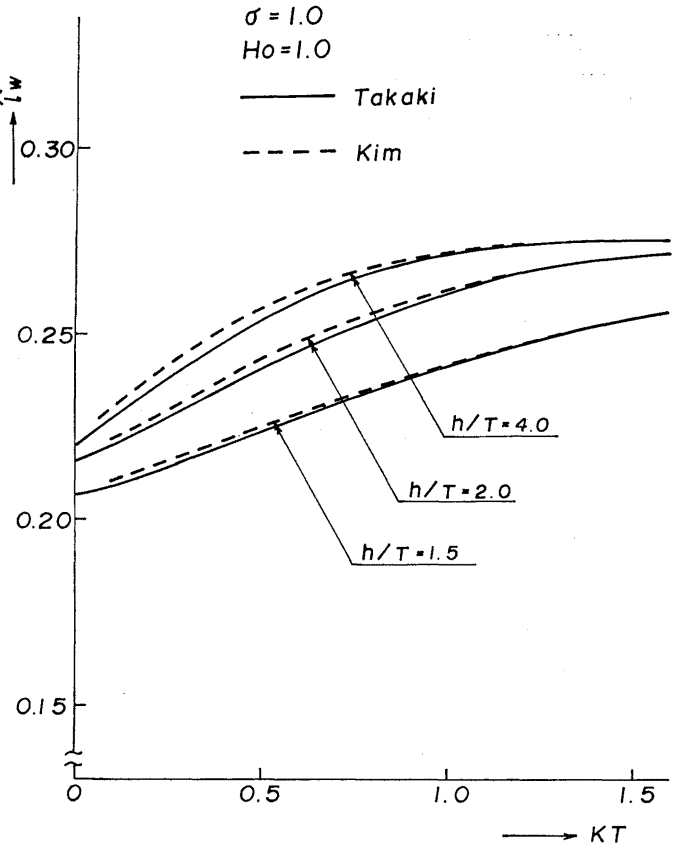

Fig. 4.43 $\hat{l}\omega$: Damping moment arm for rectangular cylinder

(ii) Semi-circular cylinder floating on a free surface of water

The added mass coefficients $\hat{M}_H$ and the wave amplitude ratios $\hat{A}_H$ for the heaving semi-circular cylinder are represented in Fig. 4.44 and 4.45 respectively, where the values in the water of infinite depth $h/T=\infty$ are obtained by the so-called "Ursell-Tasai's method."

The added mass coefficients $\hat{M}_H$ decrease in the range of low frequency as the depths of water become from the infinite depth to twice the draft of cylinder, and increase rapidly in the overall range of frequency on water depths smaller than twice the draft of cylinder. The wave amplitude ratios $\hat{A}_H$ become large throughout the range of frequency as the depths of water become shallow.

(iii) Submerged circular cylinder

According to this calculating method the hydrodynamic forces acting on the submerged cylinder can be obtained by the same method as the floating cylinder on surface of fluid. As the numerical examples the hydrodynamic forces acting on the submerged circular cylinder are shown in Fig. 4.46～Fig. 4.50. Non-dimensional coefficients of the hydrodynamic forces are expressed as follows.

$$\hat{F}_H,\ \hat{F}_S=F_H,\ F_S/2\rho g\zeta_a rL$$

$$\hat{M}_H,\ \hat{M}_S=M_H,\ M_S/\rho\pi r^2 L$$

Fig. 4.46 shows the wave exciting forces obtained by Prof. Tasai acting on the submerged circular cylinder. It is seen from this figure that the theoretically calculated values are in good agreement with his experimental results.

The added mass coefficients $\hat{M}_H$ and $\hat{M}_S$ for heave and sway increase respectively as the depths of water become shallow as shown in Fig. 4.47 and 4.49. The wave amplitude ratios $\hat{A}_H$ and $\hat{A}_S$ for heave and sway become small in the range of low frequency and large in the range of high frequency as the depths of water become shallow, where the values in water of infinite depth have been obtained by Maeda.[33] The tendency above mentioned is completely contrary to that of the floating cylinder.

It has been proved by Ursell that the heaving forces and the swaying forces acting on the submerged circular cylinder in water of infinite depth agree precisely.[34] Both hydrodynamic forces, however, do not agree because of the effect of water bottom in water of finite depth according to these calculated results.

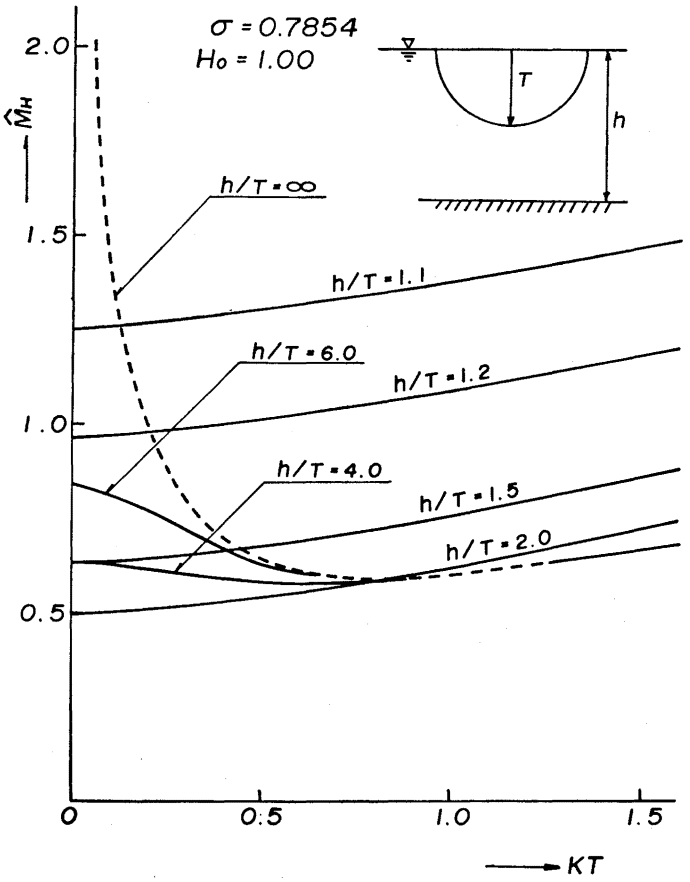

Fig. 4.44 $\hat{M}_H$: Added mass coeff. of heave for semi-circular cylinder

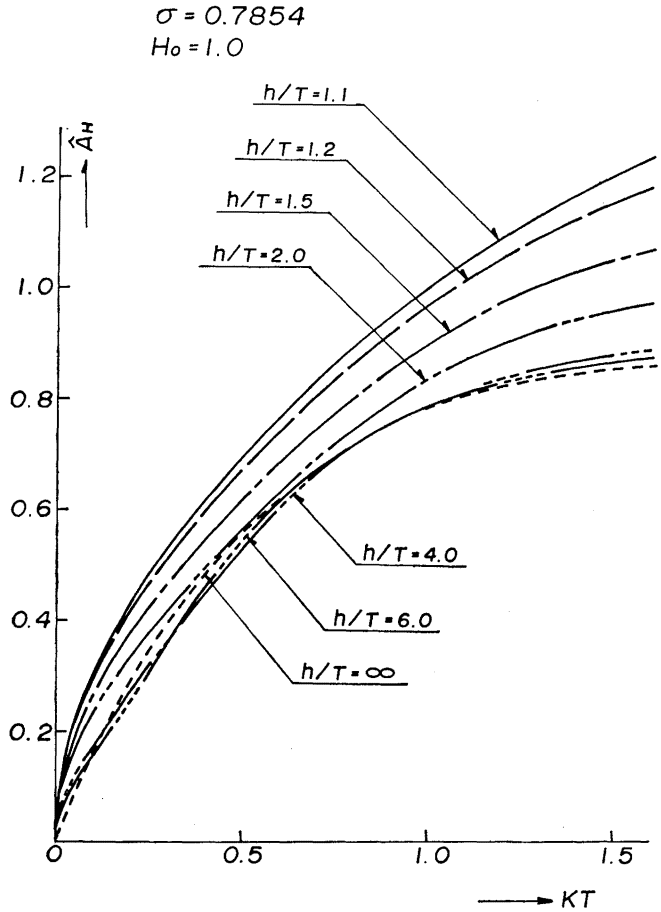

Fig. 4.45 $\hat{A}_H$: Wave amplitude ratio of heave for semi-circular cylinder

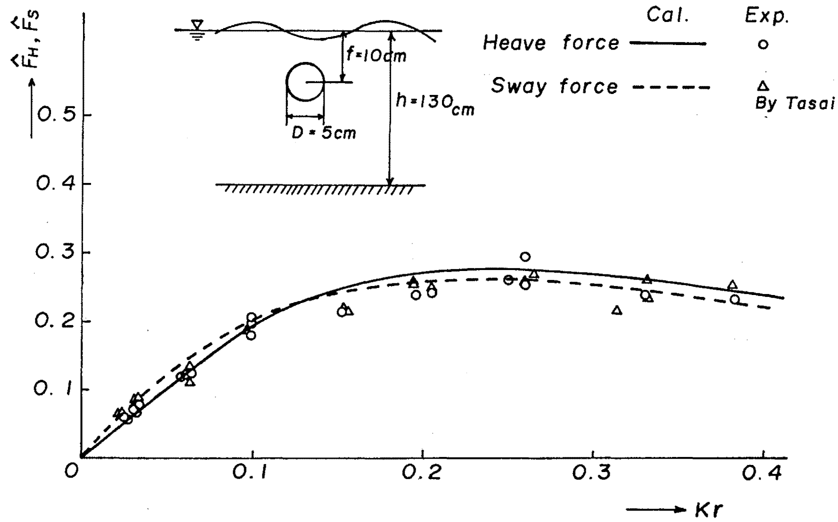

Fig. 4.46 $\hat{F}_H$, $\hat{F}_s$: Wave exciting forces acting on submerged circular cylinder

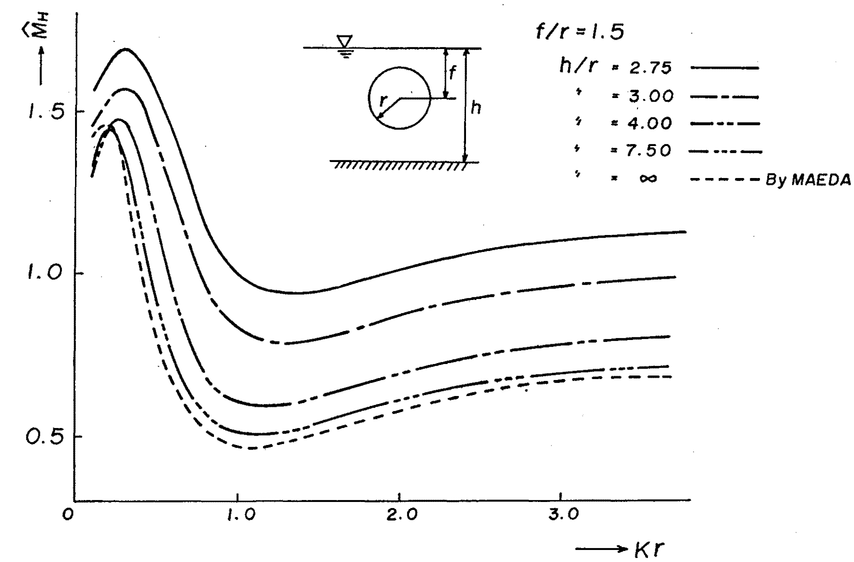

Fig. 4.47 $\hat{M}_H$: Added mass coeff. of heave for submerged circular cylinder

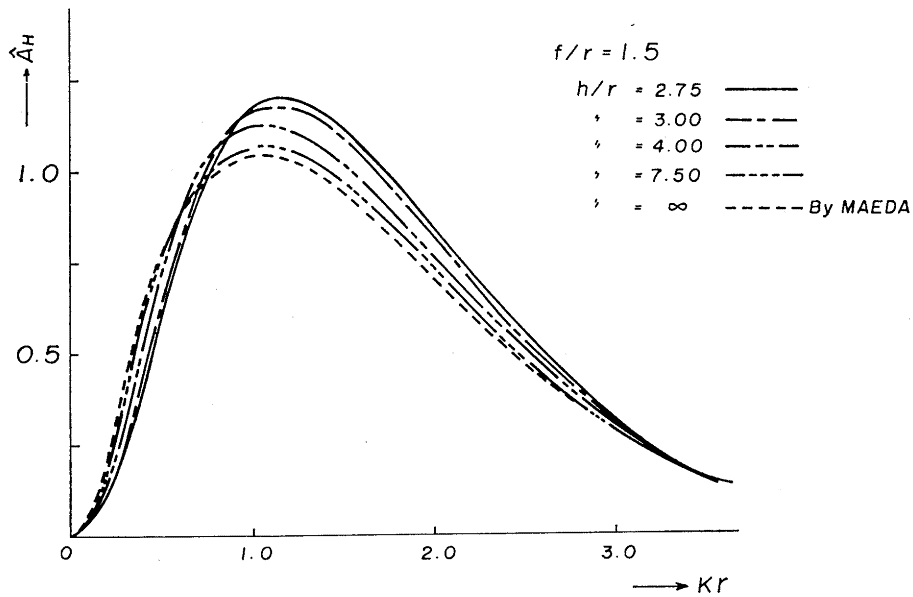

Fig. 4.48 $\hat{A}_H$: Wave amplitude ratio of heave for submerged circular cylinder

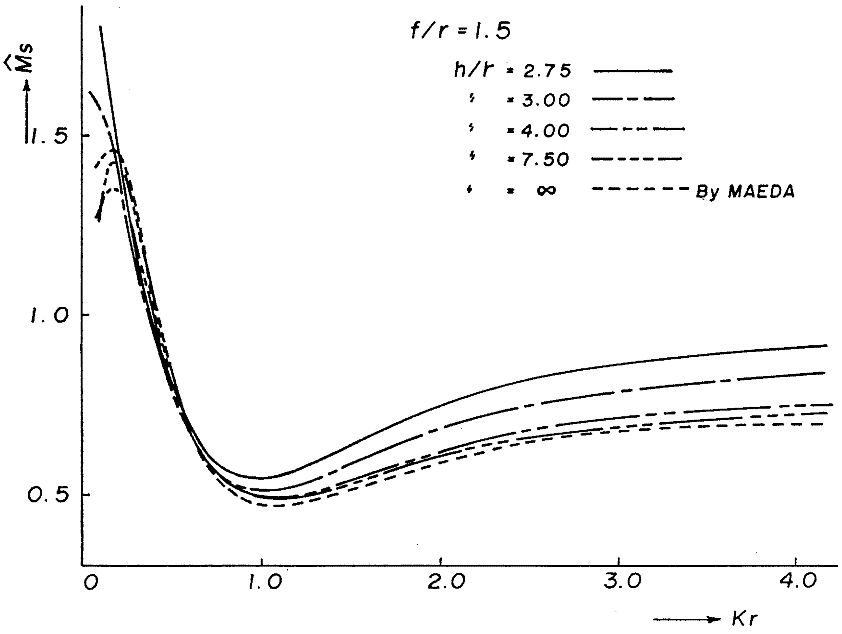

Fig. 4.49 $\hat{M}_s$: Added mass coeff. of sway for submerged circular cylinder

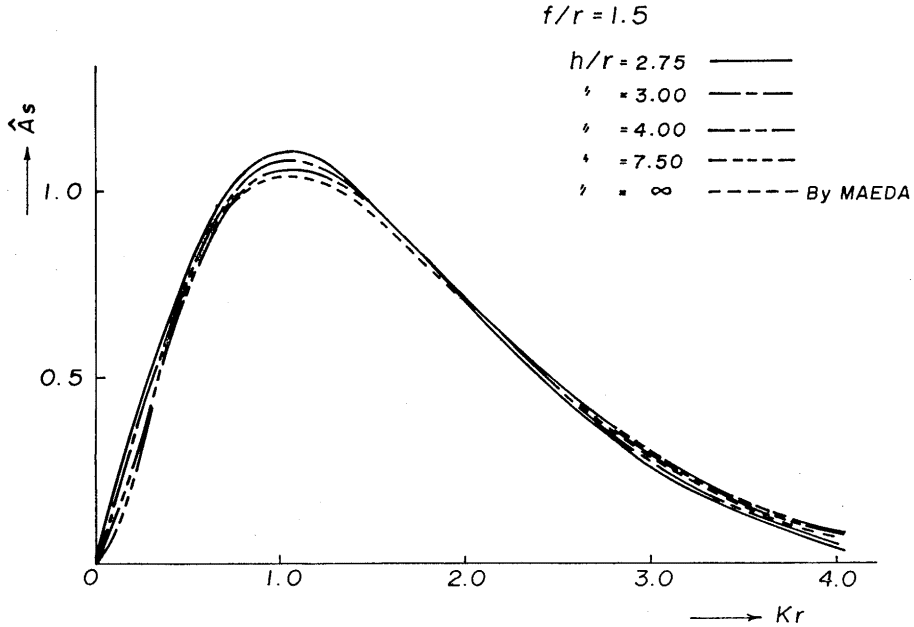

Fig. 4.50 $\hat{A}_S$: Wave amplitude ratio of sway for submerged circular cylinder

5. Conclusion

The principal purpose of the present investigations is to calculate precisely the two dimensional hydrodynamic forces and moments acting on the cylinders of arbitrary cross section in water of finite depth. The principal conclusions obtained from the results of this paper may be summarized as follows.

(1) We established a numerically calculating method for two dimensional hydrodynamic forces and moments in water of finite depth.

(2) It becomes clear from the comparison with the experimental results that the numerical calculations obtained by the above method are in good agreement with the experimental results for a naked hull without bilge-keel.

(3) It is necessary to take into account the viscous effects for added mass moment of inertia of roll in the range of low frequency as the depths of water become very shallow.

(4) The wave damping moments of rolling damping moments are affected significantly by the depths of water, however the direct forces acting on bilge-keel and the frictional damping moments are scarcely affected by the effects of water depths.

(5) The pressure distributions on the surface of the cylinder occured by the bilge-keel do not change until the water depth draft ratio is equal

to twice ($h/T=2.0$) and change very much and produce large pressure damping moments as the depth of water becomes very shallow ($h/T=1.4$).

Acknowledgement

Author is grateful to Professor F. Tasai and Associate professor M. Ohkusu of Kyushu University for their useful suggestings and encouragments and to Associate professor K. Kawatate and Associate professor W. Koterayama of Kyushu University for their valuable discussions in this work. He also wish to express his thanks to the engineer, Mr. M. Yasunaga and Mr. M. Inada for their cooperation in experiments and is indebted to Miss. M. Hojo and Miss. H. Yokobayashi for their generous assistances in preparing the manuscript.

The analysis of data were performed by means of the FACŌM 230-48 of Computer Room of Institute for Applied Mechanics in Kyushu University and the calculations of the hydrodynamic forces and moments are performed by means of the FACŌM 230-75 of the Computer Center of Kyushu University.

Reference

1) Porter, W. R., Pressure distribution, added mass and damping coefficients for cylinder oscillating in a free surface, Univ. of California, Rep. Series 82-16 July, 1960.
2) Yu, Y. S. and Ursell, F., Surface waves generated by an oscillating circular cylnder on water of finite depth: theory and experiment, J. Fluid Mech., Vol. 11, 1961.
3) Sayer, P. and Ursell, F., On the Virtual Mass at Long Wavelengths of a Half-immersed Circular Cylinder Heaving on Water of Finite Depth, Eleventh Symposium on Naval Hydrodynamics, Session V, 1976.
4) Kim, C. H., Hydrodynamic Forces and Moments for Heaving Swaying and Rolling Cylinders on Water of Finite Depth, Chalmers Univ. of Tech., Dep. of N. A. M. E., Division of Ship Hydrodynamics Rep., No. 43, April 1968.
5) Keil, H., Die hydrodynamischen Kräfte bei der peridischen Bewegung zweidimensionaler Körper an der Oberflache flacker Gewässer, Inst. Schiffbau, Hamburg, Rep. no. 305, 1974.
6) Grim, O., Eine Methode für eine genauere Berechnung der Tauch und Stamph bewegungen in glattem Wasser, H. S. V. A. Bericht No. 1217, 1960.
7) Tamura, K., The Calculation of Hydrodynamic Forces and Moments Acting on two Dimensional Body, J. of Seibu Zosen Kai, No. 26, 1963.
8) Black, J. L., Mei, C. C. and Brary, M. C. G., Radiation and scattering of water waves by rigid bodies, J. Fluid Mech., Vol. 46, Part 1, 1971.
9) Ijima, T., Tabuchi, Y. and Yumura, Y., On the Free Motions of a Floating Rectangular Body in Waves of Finite Water Depth, Technology Reports of the Kyushu Univ., Vol. 45, No. 1, 1972.
10) Bai, K. J., A Variational Method in Potential Flows with a Free Surface, College of Calif. Berkeley, Rep. No. NA72-2, 1972.
11) Bai, K. J., The added mass of two-dimensional cylindess heaving in water of finite depth, J. Fluid Mech. vol. 81, 1977.
12) Seto, H. and Yamamoto, Y., Fundamental Studies on Steady Ship Wave Problems

by the Finite Element Method, J. S. N. A. of Japan, Vol. 136, 1974.
13) Seto, H., Fundamental Studies on Steady Ship Wave Problems by the Finite Element Method (The third Report), J. S. N. A. of Japan, Vol. 141, 1977.
14) Takashina, J., Fujino, M and Yamamoto, S., Some Calculations of Hydrodynamic Forces by the Finite Element Method, J. S. N. A. of Japan, Vol. 136, 1974.
15) Maruyama, H., Fundamental Studies on the Stability of Submerged Buoyant Basement, Graduation thesis of master course in Kyushu University, 1973.
16) Kan, S., Calculation of the Two-dimensional Fluid Force Acting on a Cylinder Oscillating in Shallow Water, Paper presented at 26th General Meeting of Ship Research Institute, 1975.
17) Kan, S., Calculation of Added Mass of Two-dimensional Cylinder Oscillating in Shallow Water in Case of $K \rightarrow 0$ and $K \rightarrow \infty$, Paper presented at 28th General Meeting of Ship Research Institute, 1976.
18) Ikebuchi, T., Wave Induced Forces and Moments in Shallow Water, J. of the Kansai Society of Naval Architects, Japan, Vol. 161, 1976.
19) Bessho, M., On the Theory of Rolling Motion of Ships among Waves, Report of Scientific Research of Defence Academy, Vol. 3, No. 1, 1965.
20) Thorne, R. C., Multipole Expansion in the Theory of Surface Waves, Proc. Camb. Philos. Svc. 69, 1953.
21) Maeda, H., Wave Excitation Forces on Two Dimensional Ships of Arbitrary Sections, J. S. N. A. of Japan, Vol. 126, 1969.
22) Whittaker and Watson, A Course of Modern Analysis, Cambridge, 1927.
23) Moriguchi, S. and others, Mathematical Formulae II, p. 77, Iwanami Zensho.
24) Kan, S., Calculation of Pressure Distribution on the Surface of Two-dimensional Cylinder Oscillating Harmonically in Calm Water, Paper presented at 20-th General Meeting of Ship Research Institute, 1972.
25) Kim, C. H., Calculation of Hydrodynamic Forces for Cylinders Oscillating in Shallow Water, Chalmers Univ. of Tech., Dep. of N. A. M. E. Division of Ship Hydrodynamics Rep., No. 36, Feb., 967.
26) Kim, C. H., Effect of Mesh Size on the Accuracy of Finite-Water Added Mass, J. of Hydrodynamics, Vol. 9, No. 7, July, 1975.
27) Takaki, MI. and Tasai, F., On the Hydrodynamic Derivative Coefficients of the Equations for Lateral Motions of Ships, Transactions of West-Japan Society of Naval Architects, No. 46, 1973.
28) Tasai, F. and Kim, C. H., Effect of Shallow Water on the Natural Period of Heave, Rep. Res. Inst. Appl. Mech., Vol. XVI, No. 54, 1968.
29) Vugts, J. H., The Hydrodynamic Coefficients for Swaying, Heaving and Rolling Cylinder in a Free Surface, T. N. O. Rep., No. 194, 1968.
30) Iwai, A., Shallow Water Effect on Rolling Period of Ships in Still Water, Journal of the Nautical Society of Japan, 1966.
31) Krap, S. and Kotik, J., Wave Making Due to Tangential Forced Motion in Viscous Fluid, Preliminary Report of Researcn done by Technical Research Group, Melville, N. Y., for U. S. Navy under contract Non-361 r(100) Sep., 1963.
32) Kato, H., On the Frictional Resistance to the Rolling of Ships, J. S. N. A. of Japan, Vol. 102, 1957.
33) Maeda, H., Hydrodynamical Forces on a Cross-section of a Stationary Stracture, International Symposium on the Dynamics of Marine Viecles and Structures in Waves, 1974.
34) Ursell, F., Surface Waves on Deep Water in the Pressure of a Submerged Circular Cylinder I, Prec. Cambridge Phil. Soc. 46, 1950.

(Received Jnne 30, 1977)